Millennial-scale variations of the Holocene North Atlantic mid-depth gyre inferred from radiocarbon and neodymium isotopes in cold water corals

Christophe Colin, Nadine Tisnerat-Laborde, Furu Mienis, Tim Collart, Edwige Pons-Branchu, Quentin Dubois-Dauphin, Norbert Frank, Arnaud Dapoigny, Mohamed Ayache, Didier Swingedouw, et al.

Millennial-scale variations of the Holocene North Atlantic mid-depth gyre inferred from radiocarbon and neodymium isotopes in cold water corals

Christophe Colin[1*], Nadine Tisnérat-Laborde[2], Furu Mienis[3], Tim Collart[4], Edwige Pons-Branchu[2], Quentin Dubois-Dauphin[1], Norbert Frank[5], Arnaud Dapoigny[2], Mohamed Ayache[6], Didier Swingedouw[6], Jean-Claude Dutay[2], Frédérique Eynaud[6], Maxime Debret[7], Dominique Blamart[2], Eric Douville[2]

1. *Laboratoire GEOsciences Paris-Sud (GEOPS), UMR 8148, CNRS-Université de Paris-Sud, Université Paris-Saclay, Bâtiment 504, 91405 Orsay Cedex, France.*
2. *Laboratoire des Sciences du Climat et de l'Environnement, LSCE/IPSL, CEA-CNRS-UVSQ, Université Paris-Saclay, F-91191 Gif-sur-Yvette, France.*
3. *Royal Netherlands Institute for Sea Research (NIOZ) and Utrecht University, Den Burg, Netherlands.*
4. *Ghent University, Dept. of Geology, Ghent, Belgium.*
5. *Universität Heidelberg, Im Neuenheimer Feld 229, 69120 Heidelberg, Germany.*
6. *EPOC-CNRS, Université de Bordeaux, Allée Geoffroy Saint Hilaire, 33615 Pessac Cedex, France.*
7. *M2C, Université de Rouen, 76821 Mont-Saint-Aignan Cedex, France.*

**Corresponding author: Christophe Colin (christophe.colin@u-psud.fr).*

Abstract

Variations in North Atlantic Ocean mid-depth circulation during the Holocene are poorly understood. It is believed that they had a significant influence on the properties of water entering the Nordic Sea by redistributing heat and freshwater, potentially affecting deep-water formation and climate. To improve our knowledge of the NE Atlantic mid-depth circulation, radiocarbon and neodymium isotope analyses have been then carried out on precisely dated (U-Th) *L. pertusa* and *M. oculata* coral fragments from two sediment cores taken at ~750 m water depth on the SW Rockall Trough margin. Cold-water coral (CWC) εNd values vary between -12.2±0.3 and -16.6±0.4 and result from variable contributions of unradiogenic mid-depth subpolar gyre (mid-SPG) water (~-15) and more radiogenic Eastern North Atlantic Water (ENAW) (~-11) which is transported northward to the Rockall Trough by boundary currents along the European margin. Increased coral εNd reflects a westward contraction of the mid-SPG water and a higher proportion of ENAW. The mid-Holocene (from 8.8 to 6.8 ka BP) is marked by unradiogenic coral εNd (from -16.6±0.4 to -14.6±0.5) indicating a greater eastward extension of the mid-SPG. This is followed by a shift from 6.8 to 5 ka BP toward more radiogenic εNd

values (from -15.4±0.3 to 13.3±0.2) suggesting a westward contraction of the mid-SPG and a higher proportion of ENAW. The mid-Holocene long-term change in εNd is characterized by millennial variations of up to 2.5 epsilon units well marked during the Late Holocene, indicating that eastward extension of the mid-SPG coeval with warm periods in northern Europe (e.g. the Medieval Climatic Anomaly and the Roman Warm Period). Most of the CWC-derived $\Delta^{14}C$ values match the global ocean values indicating that the water masses bathing the corals were generally well ventilated; the exceptions are a few short intervals of eastward extension of the mid-SPG, which are characterized by lower $\Delta^{14}C$ during the late Holocene. We propose that these minor $\Delta^{14}C$ fluctuations in the Rockall Trough may be related to local changes in the mixed layer depth or to variability in the advection of water from the Labrador Sea where deep convection gives rise to thermocline waters that are relatively depleted in terms of $\Delta^{14}C$.

The eastward extension of the mid-SPG between 8.8 and 6.8 ka BP is associated with the Holocene climatic optimum, concurrent with a maximum strength of the Iceland-Scotland Overflow Water (ISOW), which is indicative of an increase in the Atlantic Meridional Overturning Circulation (AMOC). This period is followed by a transition in the North Atlantic circulation, which occurred around 6.8 ka BP, and coincides with the onset of Labrador Sea Water formation, a decrease of the ISOW strength and a contraction of the mid-SPG leading to a greater intrusion of saline subtropical water into the subpolar Atlantic.

Keywords: Cold-water corals, Rockall Trough, Holocene, Nd isotopic composition, radiocarbon, North Atlantic gyre dynamics.

1. Introduction

Although Holocene climate oscillations are small compared to the glacial and deglacial variability, their study reveals key processes controlling the natural variability of the present warm interglacial climate, which could be useful in evaluating the role of this variability in the future climate. Variations in North Atlantic Ocean surface and mid-depth circulations are controlled by the subtropical and subpolar gyres and have a significant influence on the properties of water entering the Nordic Seas by redistributing heat and freshwater. However, the Holocene variability of these North Atlantic surface and mid-depth circulations, and their link to deep water formation and atmospheric forcing, are poorly documented.

The Holocene subpolar North Atlantic climate is characterized by an early to mid-Holocene “thermal maximum” followed by progressive cooling induced by decreased insolation forcing (related to orbital precession) (e.g. Marchal et al., 2002; Sarnthein et al., 2003). This climatic cooling reflects a major reorganization of atmospheric and ocean circulation in the North Atlantic (e.g. O’Brien et al.,

1995; Came and Oppo 2007; Repschläger et al., 2017). Data- and model-based reconstructions show a change of source for North Atlantic Deep Water (NADW) production which is associated with both a decline in the production of Iceland-Scotland Overflow Water (ISOW) in the Nordic Seas during the mid-Holocene (e.g. Rasmussen et al., 2002; Renssen et al., 2005; Kissel et al., 2013; Thornalley et al., 2013) and the initiation of Labrador Sea Water (LSW) formation around 7 ka BP (Hillaire-Marcel et al., 2001; Solignac et al., 2004; Hoogakker et al., 2011, 2015).

While Holocene variability of the lower branch of the AMOC is relatively well constrained, the variations of the upper limb, which corresponds to surface and intermediate water masses transported northward by the North Atlantic gyres, are not yet well defined (Ayache et al., 2018). This is due to the complex spatial and temporal variability of the classic sea surface temperature (SST) and sea surface salinity (SSS) proxies used to track past changes in the AMOC, which are strongly influenced by the orbital-induced insolation trend and the disintegration of the residual Laurentide Ice Sheet in the Early Holocene. This leds to a pronounced provincialism in the records for surface physical properties of the North Atlantic (e.g. de Vernal and Hillaire-Marcel, 2006; Renssen et al., 2009; Eynaud et al., 2018). In addition to the long-term trend, the Holocene is marked by short-term (from centennial to millennial-scales) climate variability which is evidenced in the deep-water circulations (e.g. Bianchi and McCave, 1999; Kissel et al., 2013) and in various records throughout the North Atlantic realm (Bond et al., 1997; 2001; Debret et al., 2007; Sorel et al., 2012; Desprat et al., 2013; Smith et al., 2016).

Observations over the last few decades indicate that the North Atlantic subpolar gyre (SPG) circulation varied both in strength (Curry and McCartney, 2001; Häkkinen and Rhines, 2004, Zunino et al., 2017) and shape (Bersch, 2002; Hátún et al., 2005; Berx and Payne, 2017). These changes have played a major role in the redistribution of heat and freshwater from the surface to intermediate depths, thereby influencing the properties of waters entering the Nordic Seas (e.g. Häkkinen et al., 2011). Variations in the SPG strength and shape have been revealed by recent observations (e.g. Flatau et al., 2003; Häkkinen and Rhines, 2004). Modeling studies also highlight potential rapid changes due to internal advective positive feedback (Born et al. 2016) with a strong impact on climate (Sgubin et al. 2017). Furthermore, it has been shown that there is a close link between the SPG intensity and winds controlled by the North Atlantic Oscillation (NAO), illustrated by the downturn in the SPG circulation after the mid-1990s due to the shift from a high to low NAO index (Häkkinen and Rhines, 2004; Häkkinen et al., 2011). Over the Holocene, it has been shown that certain climatic anomalies are related to SPG intensity (e.g. Thornalley et al., 2009; Colin et al., 2010; Copard et al., 2012; Moffa-Sanchez and Hall, 2017). For instance, the warm Medieval Climatic Anomaly has been linked to a greater eastward extension of the SPG in the North Atlantic (Copard et al., 2012; Moffa-Sanchez and Hall, 2017). Conversely, the Little Ice Age has been linked to the

eastward contraction of the mid-depth SPG (Copard et al., 2012; Moffa-Sanchez and Hall, 2017). Overall, these studies have shown that SPG intensity has undergone millennial-scale changes comprising variations in the heat and salt budgets at intermediate depths, which may have influenced deep-water formation in the Nordic Seas. These millennial oscillations have been associated with a change in the main wind field resembling short-term changes related to NAO fluctuations (e.g. Copard et al., 2012; Wassenburg et al., 2016; Moffa-Sanchez and Hall, 2017; Zunino et al., 2017) even though the atmospheric pressure gradient controlling the NAO is difficult to assess at periodicities that exceed the instrumental record (Ortega et al. 2015). Reconstructing millennial scale SPG dynamics (strength and position) during the Holocene is thus necessary to provide a more comprehensive picture of the internal oscillations of the ocean and to constrain their link to the North Atlantic deep ocean circulation and climate evolution.

In this study, we have measured the Nd isotopic composition (εNd) and radiocarbon content ($\Delta^{14}C$) on precisely U-Th dated cold-water coral (CWC) fragments of *L. pertusa* and *M. oculata,* which were collected from a location in the SW Rockall Trough on the eastern edge of the SPG. Upper to mid-depth water mass circulation (above 900 m water depth) in the North Atlantic is characterized by distinct εNd values ranging from -10 for water masses originating from the subtropical Atlantic to -15 for water masses originating from the Labrador Sea (Lacan and Jeandel, 2004; Lambelet et al., 2016; Dubois-Dauphin et al., 2017). Therefore, as CWC εNd reflects the ambient seawater εNd (Copard et al., 2010; van de Flierdt et al., 2010), analyses of εNd in this archive can be used to establish the origin of the water masses (e.g. Colin et al., 2010; Copard et al., 2012; Montero-Serrano et al., 2011, 2013; Wilson et al., 2014). This has already permitted the tracking of past changes in the intensity of the mid-depth SPG (mid-SPG) in the NE Atlantic at different time scales (Colin et al., 2010; Copard et al., 2012; Montero-Serrano et al., 2011, 2013). In addition, $^{14}C/^{12}C$ measurements of U-Th dated CWC are useful for determining the age of the surrounding intermediate water mass and for reconstructing the ventilation age of the water masses (Adkins et al., 1998). The ventilation age recorded in CWC depends on (i) ^{14}C of surface water related to atmospheric ^{14}C through air-sea gas exchange and time of equilibrium between the atmosphere and water masses; (ii) the time that has elapsed since water masses reaching the CWC mounds have become isolated from the atmosphere, and (iii) vertical and horizontal mixing processes involving water masses with different ^{14}C signatures. Consequently, the combination of $\Delta^{14}C$ and εNd values analyzed on CWC samples from the SW Rockall Trough can produce a unique time series of intermediate water provenance and ventilation in the NE Atlantic.

2. Material and hydrological settings of the SW Rockall Trough

2.1 Cold-water coral samples

The CWC investigated in this study were collected from sediment cores Corals2012-39PC (55.452°N - 15.870°W, 742 m water depth; length 413 cm) and Corals2013-18PC (55.523°N - 15.644°W, 790 m water depth; length 397 cm) retrieved during the 64PE360-Corals 2012 and 64PE377-Corals 2013 cruises, respectively. In addition, one living sample of *L. pertusa* was collected with a box corer (M2000-25BX) in the same area in August 2000 (55.542°N - 15.6475°W, 773 m water depth) (Table 1 and Fig. 1). The three coring sites are located about 16 km apart on two individual carbonated mounds at the SW Rockall Trough margin (named the Logachev Mounds after the research vessel R/V Prof. Logachev) (Fig. 1; Table 1). The sediment cores are composed of biogenic fragments (mainly CWC fragments of *M. oculata* and *L. pertusa)* within a carbonate matrix. The base of core Corals2012-39PC (below 385 cm) is composed of a cemented carbonate layer associated with dropstones and volcanic glass, which have been deposited during the last glaciation (Bonneau et al., 2018). The hard-ground was not observed in core Corals2013-18PC. Only large and well-preserved specimens of *M. oculata* and *L. pertusa* were sampled. In total, 55 samples were analyzed for their Nd isotopic compositions and trace element concentrations (45 samples from core Corals2012-39PC and 10 samples from core Corals2013-18PC). In addition, a subset of 25 CWC samples from core Corals2012-39PC was selected for radiocarbon (^{14}C) analyses.

The chronological framework of the CWC samples investigated in this study is based on U-Th dating performed on the same samples and reported in Table 1 (Bonneau et al., 2018). CWC collected from cores Corals2012-39PC and Corals2013-18PC have been dated to the periods between 0.25±0.01 and 10.75±0.05 ka BP and between 1.29±0.03 and 8.65±0.09 ka BP, respectively (Table 1). Dating of CWC has revealed continuous growth of CWC throughout the Holocene. The vertical CWC accumulation rates in core Corals2012-39PC, estimated from the relationship between the U-Th age of CWC and its depth within the core, range between ~15 cm ka^{-1} and ~150 cm ka^{-1} (mean values of 33 $cmka^{-1}$) (Bonneau et al., 2018).

2.2 Hydrological settings

The cores that are the focus of this study, Corals2012-39PC and Corals2013-18PC, are located in the upper part of the permanent thermocline between a thick, sub-surface water mass and the colder, fresher LSW identified at 1200 m in the SW Rockall Trough (White and Dorschel, 2010). They are influenced by intense near-bottom currents induced by diurnal tidal movement (Mohn et al. 2014). These currents are locally important for food particle supply, replenish nutrients and oxygen to the CWC reef, and prevent the corals from being buried beneath sediments (Van Haren et al., 2014). These diurnal oscillations induce movements of the thermocline and have been highlighted by

daily temperature variations of up to ~3 °C at the thermocline depth (Van Weering et al., 2003; Duineveld et al., 2007; Mienis et al., 2007; Van Haren et al., 2014).

This setting is embedded in the large-scale cyclonic SPG circulation that characterizes the North Atlantic from the surface to at least 700 m water depth (Lavender et al., 2005). The basin-scale cyclonic SPG is defined by strong currents along the northern and western boundaries (in the northern Iceland Basin, along the Reykjanes Ridge, and in the Irminger and Labrador Seas) and a meandering North Atlantic Current (NAC) to the south (Fig. 2; Lavender et al., 2005). On the eastern boundary of the basin, the northward flow of the mid-SPG splits, with one branch flowing north into the Iceland Basin, and the other entering the Rockall Trough where an anticyclonic circulation is observed (Lavender et al., 2005).

The Rockall Trough is marked by strong wintertime mixing of the near-surface layers. This mixing reaches a depth of 500-700 m (Holliday et al., 2000) and up to 1000 m during severe winters (New and Smythe-Wright, 2001). The resulting upper-layer water mass is a mixture of saline Eastern North Atlantic Water (ENAW), which is transported poleward along the Western European margin from the Northern Bay of Biscay by the Shelf Edge Current (SEC) (Ellett et al., 1986; Pollard et al., 1996), and the fresher Modified North Atlantic Water (MNAW), which is carried by the North Atlantic Current (NAC) (New and Smythe-Wright, 2001). The MNAW is formed by the mixing of the Western North Atlantic Central Water (WNACW), which flows from the Caribbean Sea, with the Sub-Arctic Intermediate Water (SAIW), which is derived from the Labrador Current.

Below the near-surface layer, the warm, saline Mediterranean Sea Water (MSW) propagates northward along the European margin as an eastern boundary undercurrent, typically at depths of 1000-1200 m. Lozier and Stewart (2008) showed that the northward penetration of the MSW along the eastern boundary of the North Atlantic is characterized by temporal variability in relation to the NAO index and SPG expansion, implying the possibility of short-lived penetration of MSW into the eastern Rockall Trough. The inflow of Labrador Sea Water (LSW) into the Rockall Trough, characterized by a marked salinity minimum, occurs at water depths ranging from 1200 to 1900 m (New and Smythe-Wright, 2001).

Hence, CWCs collected on the Logachev Mound area are ideally located to track past changes in subpolar and subtropical water masses transported into the Rockall Trough.

3. Methods

The CWC samples were cleaned following the procedure described by Copard et al. (2010) in order to remove any sources of contamination (sediment, organic matter, Fe-Mn coatings). First, the surface of the CWC skeleton was mechanically cleaned using a diamond-blade saw in order to remove any visible Fe-Mn oxide and hydroxide coatings. The CWC fragments were further cleaned

using diluted HCl and a series of ultra-sonic baths. Dried samples were crushed into a homogeneous fraction (coarse sand grain-size) and finally divided into 3 aliquots of ~600 mg, ~50 mg and ~15 mg for Nd isotopic composition, Nd concentration and radiocarbon analyses, respectively.

3.1 Neodymium concentration and isotope analysis

Nd concentrations were measured on cleaned coral samples (20–30 mg), dissolved in supra-pure 3 N HNO_3, using a quadruple ICP-MSXseriesII (Thermo FisherScientific) at the Laboratoire des Sciences du Climat et de l'Environnement (LSCE, France) and following the procedure described in Montero-Serrano et al. (2013). Briefly, sample and standard solutions were systematically adjusted at 100 ppm Ca through dilution, without further chemistry. To compensate signal derivation by a few percent during a day, a standard (JCp-1) was run every five samples. Instrumental bias was taken into consideration by a bracketing technique giving an analytical uncertainty of 5% (2σ) for Nd concentrations.

Nd was purified from cleaned coral samples (~600 mg) using Eichrom TRU-Spec and Ln-Spec resins following the detailed analytical procedures described in Copard et al. (2010). The $^{143}Nd/^{144}Nd$ ratios were analyzed using the ThermoScientific Neptune^{Plus} Multi-Collector Inductively Coupled Plasma Mass Spectrometer (MC-ICP-MS), hosted at the LSCE. The bracketing correction method outlined by Dubois-Dauphin et al (2017) was applied. For the Nd isotope analyses, sample and standard concentrations were matched at 4 to 10 ppb. Mass-dependent fractionation was corrected by normalizing $^{146}Nd/^{144}Nd$ to 0.7219 and applying an exponential fractionation law. During the analytical sessions, every set of two samples was bracketed by analyses of the La Jolla Nd standard solution, which is characterized by certified values of 0.511858±0.000007 (Lugmair et al., 1983). The offset value between results and certified values of La Jolla was inferior to 0.4 εNd units for all of the analyses presented in this study. The analytical errors reported herein correspond to the external two sigma standard deviation (based on repeat analyses of the La Jolla standard for the different analytical sessions). For a few coral samples the internal two sigma standard deviation is used as it is higher than the external two sigma standard deviation. The analytical errors obtained ranged from 0.2 to 0.5 epsilon units (Table 1). The analytical blank values for Nd were <4 pg, which represents less than 0.1% of the minimum Nd yield from CWC skeletons used in this study. As a result no blank correction was applied.

3.2 Radiocarbon dating

Approximately 15 mg samples of clean coral powder were treated with 0.01N HNO_3 for 15 min, rinsed with MilliQ water and dried. Each sample was then converted to CO_2 in a semi-automated carbonate vacuum line (Tisnérat-Laborde et al., 2001). The CO_2 was reduced into graphite

using hydrogen in the presence of iron powder. Accelerator mass spectrometry (AMS) ^{14}C dating was performed using the AMS equipment at ARTEMIS (LM14C - Saclay, France, Cottereau et al., 2007). Blanks were obtained on a *L. pertusa* sample older than 100 000 yrs (U-Th age), and yielded a mean activity of 0.0022 $F^{14}C$ (apparent age older than 48 000 yrs). Radiocarbon results are reported as conventional ^{14}C ages in yr BP and in terms of $\Delta^{14}C$ defined as the per mil (‰) deviation of a sample's $^{14}C/^{12}C$ ratio from that of a 19th century wood standard after correction of blank, fractionation and correction for decay obtained from U-Th ages (cal yr BP) (Stuiver and Polach, 1977) (Table 1). The marine reservoir ages (R) were calculated as the offset of the measured ^{14}C age of coral from contemporaneous atmospheric ^{14}C age based on IntCal13 (Reimer et al., 2013). The reservoir offsets (ΔR) were estimated by calculating the difference between the marine radiocarbon age of surface water based on the Marine13 curve and the ^{14}C age of coral at that same time.

4. Results

The Nd concentrations obtained for fossil deep-sea corals of both cores, Corals2012-39PC and Corals2013-18PC (*L. pertusa* and *M. oculata*), range from 7.1 to 55.0 ppb (Table 1). Such range of Nd concentrations are in accordance with Nd concentrations previously obtained on CWC from the SW Rockall Trough (7.3-184.3 ppb) (Colin et al., 2010; Copard et al., 2012). Copard et al. (2010) have shown that such Nd concentration ranges are not linked to the presence of Nd contamination from manganese-oxide and iron hydroxide coatings. Struve et al. (2017) have recently suggested that authigenic phosphate phases (hypothesized apatites) could be important carriers of skeletal Nd in cleaned CWC. This could explain the large range of Nd concentrations observed on the aragonite skeleton.

One living sample of *L. pertusa* collected in box core M2000-25BX in August 2000 provides an εNd of -13.6±0.4 (Table 1), which is indistinguishable from ambient seawater εNd of -13.5±0.2 (Dubois-Dauphin et al., 2017; Fig. 2a). This finding confirms that cleaned CWC skeletons record ambient seawater εNd (Copard et al., 2010; van der Flierdt et al., 2010).

εNd obtained on *L. pertusa* and *M. oculata* collected from Corals2012-39P and Corals2013-18PC range from -12.2±0.3 to -16.6±0.4 (Table 1). The coral εNd records display a decreasing trend (from -13.2±0.2 to -14.9) between 10.7 and 9.1 ka BP. The time interval from 8.8 to 6.8 ka BP is associated with low εNd values (from -14.3±0.5 to -15.4±0.3) and is followed by a progressive increase of the εNd from -15.4±0.3 to -13.3±0.2 during the time interval between 7 and 5 ka BP. One coral sample dated to 8.6 ka BP displays an unradiogenic εNd value of -16.6±0.4. The interval spanning the last 5 ka BP is marked by more radiogenic εNd values ranging from -14.3±0.2 to -12.2±0.3.

Coral εNd values obtained in this study are combined with published data from CWC fragments collected from several carbonate mounds within a limited area of the SW Rockall Trough and at a similar water depth (between 725 and 790 m water depth) (Colin et al., 2010; Copard et al., 2012) (Fig. 2). This new dataset, presented in Figure 3, is composed of 100 coral εNd values spanning the last 11 ka. The new results reproduce the variability observed in the previous coral εNd record (Colin et al., 2010), thus confirming the large-scale character of Nd isotope changes in the SW Rockall Trough. The new data imply a roughly twofold increase of time resolution compared to existing Holocene coral εNd data from the Rockall Trough. Nevertheless, the time resolution is variable throughout the Holocene, with lower resolution before 6 ka BP due to marked changes in CWC abundance at the SW Rockall Trough margin (Bonneau et al., 2018). The Early Holocene (between 8.8 and 6.8 ka BP) stands out as period with unradiogenic εNd values. Our new CWC εNd stack confirms a mid-Holocene transition from subpolar to subtropical Nd isotopic signatures (Colin et al., 2010), but shows that this transition was rather smooth (lasted ~1.5 ka) and started just after 7 ka BP. Superimposed on this long-term trend, millennial variations in the coral εNd of up to 2.5 epsilon units can be identified, especially during the Late Holocene (Fig. 3).

The $\Delta^{14}C$ results obtained from CWC in this study (Table 1) plotted against U-Th dates, are compared with the IntCal13 and Marine13 $\Delta^{14}C$ calibration curves (Reimer et al., 2013) from 0 to 10.1 ka BP and range from -72±4 ‰ to +70±9 ‰ (Fig. 3). The decrease of CWC-derived $\Delta^{14}C$ observed between the Early and Late Holocene is consistent with the Marine13 curve and is mainly linked to the decrease of atmospheric $\Delta^{14}C$. Most of the CWC-derived $\Delta^{14}C$ values match the Marine13 $\Delta^{14}C$ calibration curve.

Eight CWC-derived $\Delta^{14}C$ values differ from the Marine13 calibration curve. These differences are significant at 2 sigma according to the Chi-square test at a 95% significance level. One sample (CWC sample from core Corals2012-39PC at 137.5 cm) yielded a higher $\Delta^{14}C$ value at 3.67 ka BP (-1.6 ± 5‰), which corresponds to an enrichment of 20 ‰ compared to the Marine13 curve at this time (-21.5 ± 3.2 ‰). Seven CWC samples (CWC samples from core Corals2012-39PC at 38.5, 87.5, 109.5, 120.5, 169.5, 227.5 and 241.5 cm), whose respective ages are centered at 6.1, 4.4, 2.7, 2 and 0.7-1 ka BP, are characterized by $\Delta^{14}C$ values that are lower than the Marine13 $\Delta^{14}C$ calibration curve (red arrows in figure 3). In two cases, at about 6.1 ka and 2.7 ka BP, two CWC samples, results confirm this decreasing trend in $\Delta^{14}C$. The lower $\Delta^{14}C$ (Fig. 3) values correspond to an older ^{14}C age for water and thus reflect an increase in the marine reservoir age, which reaches up to 519±35 years (Table 1). The marine reservoir ages of these seven CWC samples are characterized by a mean value of 475 years (n=7), which is higher than the mean reservoir age obtained on the other CWC samples investigated in core Corals2012-39PC (367 years; n=18).

5. Discussion

5.1. Oceanographic controls on Rockall Trough seawater εNd

Two recent studies have provided new insights into the signature of the seawater Nd isotopic composition in the eastern (Dubois-Dauphin et al., 2017) and western (Lambelet et al., 2016) North Atlantic. Seawater εNd is found to be homogeneous (between -14 and -15) throughout the SPG for the upper 1500 m water depth, suggesting a similar origin for the surface to intermediate subpolar waters (Lambelet et al., 2016; Dubois-Dauphin et al., 2017). Likewise, the upper 1500 m of the Rockall Trough water column are characterized by homogenous Nd isotopic compositions (from -14.0±0.2 to -13.3±0.2; Dubois-Dauphin et al., 2017) (Fig. 2b). Thus, subsurface to intermediate water masses are largely indistinguishable on the basis of their Nd isotope characteristics. Nevertheless, when compared to εNd values for the SPG, those from the Rockall Trough seem to be influenced by a more radiogenic end-member (Fig. 2b). Recent results obtained by Dubois-Dauphin et al. (2017) along a North-South transect at 25°W, spanning the SPG and sub-tropical gyre (STG) interface, highlight that water masses carried by the NAC from the surface to ~900 m water depth have an unradiogenic Nd isotopic signature (from -15.1±0.3 to -13.8±0.3; Dubois-Dauphin et al., 2017). This implies that MNACW εNd is strongly influenced by SAIW originating from the Labrador Sea, with dissolved Nd concentrations that are twice those of WNACW in the western STG (Lambelet et al., 2016). Consequently, this indicate that coral εNd record of the SW Rockall Trough cannot be interpreted by a modification of proportions of water masses from SPG and STG waters transported in the NAC as it was proposed by Colin et al. (2010). The more radiogenic end-member εNd observed in the Rockall Trough can be only due to the contribution of the radiogenic NEAW which is transported northward by the SEC (εNd signature of -11.3±0.4 in the Bay of Biscay, 1σ, n=6; Rickli et al., 2009; Copard et al., 2011). In addition, at greater water depth (around 950 m), the radiogenic MSW (εNd around -10.6±0.3; Dubois-Dauphin et al., 2017) is also carried northward along the western European margin to the Porcupine Seabight (Dubois-Dauphin et al., 2017). The presence of MSW in the Eastern Rockall Trough has been shown to respond to the dynamics of the mid-SPG, such that mid-SPG contraction induces northward penetration of MSW (Lozier and Stewart, 2008). Hence, by vertical mixing and recirculation (Holliday et al., 2000; Lavender et al., 2005) the MSW could also induce a more radiogenic εNd signature to intermediate water masses of the Rockall Trough.

In summary, εNd values of intermediate waters at the SW Rockall Trough result mainly from the mixing of unradiogenic MNACW (εNd from -15.1±0.3 to -13.8±0.3), which was carried by the NAC, and radiogenic ENAW (εNd ≈ -11.3) and MSW (-10.6±0.3), which propagated northward along the European margin. Consequently, mid-depth coral εNd records from the SW Rockall Trough can be

linked to the spatial evolution of the interface between the mid-SPG waters and the ENAW/MSW carried northward by the European slope current. An eastward expansion (westward contraction) of the mid-SPG will induce a decrease (increase) in the relative proportion of the ENAW/MSW resulting in unradiogenic (radiogenic) Nd isotopic signatures for intermediate water masses in the Rockall Trough.

5.2. The reorganization of mid-depth circulation in the North Atlantic during the Holocene

The coral εNd record for the SW Rockall Trough displays significant variations, ranging from -12.2±0.3 to -16.6±0.4, over the Holocene, marked by a shift towards less mid-SPG influence between 7 and 5 ka and punctuated by abrupt events. Howe et al. (2016) suggested that increased detrital input from the Laurentide Ice Sheet in the Early Holocene (Kurzweil et al., 2010) induced a modification of the εNd of deep-water masses of the North Atlantic, which is well marked in cores located at water depths greater than about 2500 m. Holocene seawater εNd records for the intermediate water of the Labrador Sea are not available but we cannot rule out the possibility that the εNd of the SPG had also been modified at the beginning of the Holocene. Nevertheless, variations in the coral εNd of the SW Rockall Trough cannot be explained solely by changes in the Nd isotopic composition of the water masses induced by lithogenic input from the Laurentide Ice Sheet for several main reasons. First, whereas melting of the Laurentide Ice Sheet was greater in the early Holocene than during the mid-Holocene, CWC εNd from the SW Rockall Trough is slightly more radiogenic in the early Holocene than the mid-Holocene (time interval from 8.8 to 6.8 ka BP). Second, observations of unradiogenic εNd from the early Holocene occur mainly at abyssal depths (around 4500 m, Howe et al., 2016), and are less clear at depths corresponding to NADW. Radiocarbon results suggest fairly well-ventilated water (predominantly thermocline down to modern LSW) and hence indicate little influence from abyssal ($\Delta^{14}C$ depleted) waters at our site. The variability we observe in coral εNd is thus much more likely to be related to changes in the upper water column which, according to Howe et al. (2016), does not seem to be as affected by this detrital input. Third, late Holocene variations in coral εNd are of a similar magnitude (up to 2.5 epsilon units) as the early/middle Holocene, but these late Holocene variations cannot be explained by lithogenic input because the final demise of the Laurentide Ice Sheet occurred earlier (around 6.8 ka, Carlson et al., 2008). Finally, the studied site is located on the eastern edge of the SPG implying marked variations in the relative proportion of water masses from the SPG flowing into the SW Rockall Trough.

Therefore, based on the assumption that the sources of Nd for the water masses are constant throughout the Holocene (i.e. taking into account the εNd and salinity of pure end-member mid-depth waters from the SPG and STG), it is possible to estimate a salinity range at mid-depth of

about 1 PSU (from 35.0 to 36.0). This is in agreement with the range of Holocene sub-thermocline salinity estimated from coupled Mg/Ca-$\delta^{18}O$ measurements obtained for planktic foraminifera from the South Iceland Rise by Thornalley et al. (2009). Assuming constant εNd end-members for the mid-depth SPG (-15) and STG (-11), we can estimate that the contribution of the SPG to the Rockall Trough intermediate waters varied from around 20% (80% STG) to 100% (no influence of the STG) over the last 11 ka. Our results confirm that the Early Holocene, between 8.8 and 6.8 ka BP, was marked by an eastward expansion of the mid-SPG, compared to present-day conditions, in agreement with Thornalley et al. (2009) (Fig. 4c). In addition, planktonic faunal assemblages (such as *G. inflata* % reported in Fig. 4d) and oxygen stable isotopic records obtained on cores located in the surroundings of the Faroe Islands suggest an eastward expansion of the NAC and reduced contributions of warm saline waters from the STG to the Nordic Sea from 8 to 6 ka BP (Staines-Urias et al., 2013). These results suggest that, between 8 and 6 ka BP, the upper layer of the NE Atlantic was characterized by cold, fresh water implying an eastward extension of the SPG, which, at mid-depth, is consistent with the high contribution of water originating from the mid-SPG estimated on the basis of CWC εNd in the SW Rockall Trough.

Most of the $\Delta^{14}C$ values for CWC from the SW Rockall Trough are similar to those of the Marine13 $\Delta^{14}C$ calibration curve indicating that the water surrounding the corals remained relatively well ventilated, particularly before 6 ka BP (Fig. 3). The Li/Mg temperature record of the mid-depth waters obtained by Bonneau et al. (2018) on the same CWC samples as those investigated in this study is reported in the Figure 3 with a view to comparing it to εNd and $\Delta^{14}C$ records (Fig. 3). Whilst the εNd record indicated large-amplitude changes in the water mass origin, Li/Mg reconstructed temperatures exhibit relatively low variability (from 7 to 9°C) during the Holocene (about 2°C). This may imply that winter convection was at least as deep as it is now (between 500 to 1000 m water depth; Holliday et al., 2000; New and Smythe-Wright, 2001) without drastic changes in the vertical temperature distribution. Nevertheless, the slightly lower Li/Mg temperature (7.0±0.9 to 7.9±0.9 °C) observed in the Early Holocene (before 6 ka BP), compared to the Late Holocene (7.4±0.9 to 8.8±0.9 °C) (Bonneau et al., 2018), may be compatible with a greater proportion of colder SAIW (Pollard et al., 1996) as is observed in the CWC εNd record for the SW Rockall Trough.

5.3. Implications of the mid-Holocene long-term variations in SPG intensity on ISOW formation and on εNd of the deep-ocean

Only a handful of studies have addressed the evolution of the deep-limb of the AMOC in the subpolar North Atlantic during the Holocene (e.g. Bianchi and McCave, 1999; Praetorius et al., 2008; Kissel et al., 2013; Thornalley et al., 2013; Howe et al., 2016; Ayache et al., 2018). These studies have identified several short-term variations in the intensity of North Atlantic deep-water, with amplitude

and timing depending greatly on the region investigated and the proxies used. Thornalley et al. (2013) presented a stacked sortable silt record from the Reykjanes Ridge, which is indicative of the Iceland–Scotland overflow strength during the Holocene. In figure 4b, we present the stacked sortable silt record for comparison with the CWC εNd record (Fig. 4f). Results reveal a decrease in Iceland-Scotland Overflow Water (ISOW) strength during the Mid- to Late Holocene, with maximum Iceland–Scotland overflow strength occurring at ~7 ka; this maximum corresponds to low CWC εNd values in the SW Rockall Trough. This suggests a link between the position of the mid-SPG and the strength of the Iceland–Scotland overflow, which forms an important component of the deep branch of the AMOC (Figs. 4b and 4f). In addition, to overcome complex spatial and temporal variability of the classic SST and SSS proxies strongly influenced by the orbital-induced insolation trend and the disintegration of the residual Laurentide Ice Sheet in the Early Holocene, Ayache et al (2018) have extracted significant AMOC mode variations based on a relatively large compilation of paleo-ocean SST data (HAMOC database; Eynaud et al., 2018) from the North Atlantic Basin. They have identified a period of enhanced AMOC mode in the period between 8 and 6.5 ka BP, which is associated with a greater extension of the mid-SPG (low coral εNd). This period of intensified AMOC is followed by a general weakening trend from around 6–7 ka to 2 ka, which is also consistent with the progressive westward contraction and weakening of the mid-SPG observed in the Rockall Trough after 7 ka BP.

Before ~7 ka BP, water masses originating from the Labrador Sea were advected at lower water depths (Hillaire-Marcel et al., 2013) and may have been linked to the surface and sub-surface layers. These water masses may have entrained unradiogenic Nd isotopic composition from the surface water of the Labrador Sea, which is marked by boundary exchange (Lambelet et al., 2016). At intermediate depth (above 1000 m), we suggest that an intense SPG circulation would have brought a greater volume of seawater into contact with the unradiogenic sediments of the Labrador Sea and the Greenland margins (Jeandel et al., 2007). Thus, it is possible that such an intensification of SPG circulation could also have increased the lithogenic Nd input from the boundary exchange. Such increase of lithogenic Nd input needs then to be taken into account in the budget of Nd input to the North Atlantic.

Today, the SPMW and LSW are entrained and mixed with the ISOW within the Iceland–Scotland overflow. This entrainment of surrounding waters characterized by unradiogenic εNd values modifies the pure ISOW signature (-8.2±0.6; Lacan and Jeandel, 2004) to a value of -10.5±0.5 after overflowing the Iceland-Faroe ridge (Dubois-Dauphin et al., 2017). Based on εNd values and salinity, Dubois-Dauphin et al. (2017) have estimated that ISOW flowing in the Iceland Basin is composed of

~60% pure ISOW and of 40% entrained surrounding waters (LSW ε_{Nd}= -13.9±0.4; and Modified North Atlantic Water -MNAW εNd= -13.1±0.3; Lacan and Jeandel, 2005). The time interval from 8.8 to 6.8 ka BP is associated with an eastward extension of the mid-depth (CWC εNd of the SW Rockall Trough) and surface SPG (Thornaley at al., 2009; Staines- Uria, 2013). This increased flow of surface and sub-surface waters, characterized by unradiogenic Nd isotopic signatures, in the Iceland basin may then have been entrained by an intense ISOW (Thornaley et al., 2013). This thus would have contributed, along with the Nd lithogenic input from detrital material of the Laurentide Ice Sheet (Howe et al., 2016), to the unradiogenic Nd signature observed for the NADW in the Early Holocene in several deep sites of the North Atlantic (Roberts et al., 2010; Böhm et al., 2015; Howe et al., 2016; Lippold et al., 2016). Further modeling studies of the Nd isotopic composition are required in order to better evaluate the lithogenic Nd inputs to the subpolar water and its impact on the Nd isotopic signature of the North East Atlantic Deep Water (NEADW) during the Early Holocene through the entrainment of SPMW deriving from an intensified SPG, into the ISOW.

5.4. Millennial scale variations of the mid-SPG

The coral εNd record shows several short periods of eastward extension (low coral εNd values), which occurred approximately every 1500±500 years, centered around 10.1, 8.6, 5.5, 4.5, 2.5, 1.8 and 0.8 ka BP (Fig. 3). For the Late Holocene, some of these time intervals (centered at 6.1, 4.4, 2.7 and 0.7-1 ka BP) are also associated with $\Delta^{14}C$ values that are 14 to 20‰ lower than the Marine13 curve (Fig. 3). These differences, which are statistically significant, correspond to higher marine reservoir ages that are between 430±30 and 519±35 yrs (Table 1). This millennial-scale climate variability during the Holocene was first pointed out by Bond et al. (1997 and 2001) (1470±500-year cycles) and is related to a combination of solar activity (1000 and 2500-year cycles) and AMOC internal variations (1500-year cycles), which are particularly well marked for the last 5 ka (Debret et al., 2007). This late Holocene time interval is also associated with large variations in the CWC εNd record obtained on the SW Rockall Trough (Figure 3).

Several processes may be responsible for the recorded $\Delta^{14}C$ variability. First, the $\Delta^{14}C$ variability may also be directly related to the changes in the relative advection of thermocline water from the SPG (i.e. SAIW) and STG. Modern observations (pre-industrial ^{14}C estimates in GLODAP v1.1; Key et al., 2004) and modeling studies covering the Holocene (Franke et al., 2008; Butzin et al., 2017) indicate the existence of a considerable offset in radiocarbon contents between these sources. The poorly stratified SPG is thoroughly mixed by deep convection resulting in the upper water having a bomb-corrected $\Delta^{14}C$ of -65‰ (Key et al., 2004) and reservoir ages of around 550 ^{14}C years (Butzin et al., 2017), which is slightly depleted/older with respect to modern global surface ocean (-58‰ and 470 ^{14}C years of Marine13; Reimer et al., 2013). In contrast, the stratified thermocline water in the

STG is well equilibrated to the atmosphere, with modern surface $\Delta^{14}C$ of -45‰ (Key et al., 2004) and reservoir ages of 300 ^{14}C years (Butzin et al., 2017) which is less depleted/younger than the average modern surface ocean (Marine13; Reimer et al., 2013). Furthermore, in the modern ocean the anomalous ^{14}C enriched water from the upper STG is observed to follow the NAC towards the European Margin and the Rockall Trough (Key et al., 2004). The variability of $\Delta^{14}C$ relative to the Marine13 curve observed in Rockall Trough coral record is of a similar magnitude as the offset between the gyres and thus may simply be caused by changes in the relative advection of STG and SPG thermocline waters as indicated by the coeval εNd excursions (Fig. 3). Analogous radiocarbon variability related to dynamic changes in the STG influence has also been recorded in several shallower records downstream from the Rockall Trough (Ascough et al., 2009; Eiríksson et al., 2011; Wanamaker Jr et al., 2012).

However, given the position of the corals near the base of the modern mixed layer (Holliday et al., 2000; New and Smythe-Wright, 2001), local variability in the mixed layer depth throughout the Late Holocene may have driven the observed variability in radiocarbon contents. Over the last decades, mixed layer depth has varied significantly in the Rockall Trough region and appears to be principally forced by the position of the NAC and hence the extent of the SPG (Carton et al., 2008). Wade et al. (1997) proposed that the SAIW, which is characterized by low salinity and temperatures (4°C - 7°C, 34.7-34.9 PSU, Pollard et al., 1996) underneath the Central Water, plays an important role in the stability of the NE Atlantic water column. They demonstrated that the presence of relatively 'pure' SAIW in the NE Atlantic prevents deep winter mixing due to enhanced stratification. In contrast, the absence of a well-defined SAIW layer induces a weaker density gradient allowing deep winter convection (Ellett et al., 1986; Holliday et al., 2000). As such, the incursion of SAIW in the Rockall Trough during the Late Holocene episodes of SPG expansion, as indicated by unradiogenic coral εNd, may have shoaled the mixed layer depth. The water masses around the studied CWC can be then isolated from upper waters resulting in the observed $\Delta^{14}C$ depletion with respect to the surface ocean (Marine13 $\Delta^{14}C$ calibration curve; Reimer et al., 2013).

Finally, the observed radiocarbon variability may also have originated from perturbations of the convection processes in the Labrador Sea. Between 1885 and 1950 AD, $\Delta^{14}C$ fluctuations of 10‰ to 18‰ occurred in the surface of the NE Atlantic Ocean (Tisnérat-Laborde et al., 2010). They may have originated in the Labrador Sea through the increased vertical convection and formation of SPMW due to reinforced wind strengths in the high latitudes of the North Atlantic, as suggested by Reverdin et al. (1997) for SSS anomalies. The surface freshwater intrusion in the Labrador Sea inhibits deep convection as was observed during the great salinity anomaly in the 1960s (Reverdin et al., 1997; Swingedouw et al. 2015). The demise of the Laurentide Ice Sheet ended at around 6.8 ka BP, but several meltwater peaks are identified during the Late Holocene in the Labrador Sea and are

mainly attributed to the melting of the Greenland Ice Sheet (Fig. 4a) (Hoogakker et al., 2015). Taking into consideration the error in age models, the $\delta^{18}O_{seawater}$ curve at Orphan Knoll (Labrador Sea) (Fig. 1) displays several events of SSS increase at about 4.2, 2.4, 1.8, and 1.0 ka BP (Hoogakker et al., 2015) which correspond to an extension of the SPG (low coral εNd) (Figs. 4a and 4f). Such results are consistent with a scenario where less freshwater input by the Eastern Greenland current to the Labrador Sea could be responsible for a millennial perturbation of the LSW formation and SPG circulation (Moffa-Sanchez and Hall, 2017). In this scenario, a decrease in freshwater input to the Labrador Sea would enhance vertical convection resulting in relatively ^{14}C depleted upper SPG waters (SAIW). Episodes of eastward extension of the SPG (low CWC εNd) may thus be responsible for the advection of more ^{14}C-depleted SAIW in the SW Rockall Trough during the Late Holocene, in agreement with our radiocarbon results. Further investigations will be necessary to constrain the variability of the reservoir age within the subpolar Atlantic during the Holocene.

In summary, the relatively small $\Delta^{14}C$ variations recorded in the Rockall Trough do not allow us to distinguish between these potential processes. Nonetheless, all processes highlight the important role of the SPG dynamics which is consistent with the εNd record.

The intervals of eastward extension of the mid-SPG are not systematically correlated to those inferred from SST and SSS reconstructions for surface and sub-surface water masses to the south of Iceland by Thornalley et al. (2009); exceptions are the Early Holocene event involving the significant eastward extension of SPG (between 9 and 6.8 ka BP) and the short events labeled 0, 1 and 2 in figures 4c and 4f. Whereas SSS only records the evolution of inter-gyre mixing linked to the shape and intensity of the SPG, the mid-depth εNd record also tracks the northward intrusion of the ENAW by boundary current along the European margin. Nevertheless, both records are highly sensitive to the shape and intensity of the SPG but they do not strictly match each other. According to Miettinen et al. (2012) a regional SST see-saw exists between the Norwegian Sea and the subpolar North Atlantic and is clearly identified for the LIA – MWP climate periods. This was associated with a marked rerouting of the eastern and western branches of the surface limb of the AMOC (NAC) in the NE Atlantic (Miettinen et al., 2012) giving rise to SST and SSS records which are not synchronous. Nevertheless, the lack of regional synchronicity for short events, especially when they are derived from SST records, has been pointed out in many studies (e.g. Larsen et al., 2013) and could be linked to characteristics of the NAO itself (Miettinen et al., 2012).

The time interval from 1 to 0.68 ka BP, which is marked by a strong eastward extension of the SPG, has been associated with the warm Medieval Climatic Anomaly and a subsequent intensification of the surface limb of the AMOC (Copard et al., 2012; Wanamaker et al., 2012; Ortega

et al., 2015) (Fig. 4). The westward contraction of the weak SPG observed thereafter (between 0.68 and 0.2 ka BP) is coeval with the cold period of the Little Ice Age and may be linked to reduced AMOC intensity. Furthermore, compared to the εNd values of CWC dated between 90 and 800 yrs BP (-12.8 on average; n=19), the unradiogenic εNd of modern CWC (dated to the last 50 years; -13.6 on average, n=15) as well as that of seawater (Fig 2a) (-13.5 at 700 m in the Rockall Trough; Dubois-Dauphin et al., 2017) suggest a greater extension of the mid-SPG during the last century (labeled as event 0 in Figure 4f). This could be associated with global warming induced by considerable anthropogenic greenhouse gas emissions and is consistent with an enhanced heat and salinity flux to the Arctic Ocean supplied by the NAC (Spielhagen et al., 2011). The new εNd value record indicates several other periods of major eastward extension of the SPG suggesting a strong millennial variability in the intensity of the surface limb of the AMOC (Fig. 4f). The time interval between 2.1 and 1.7 ka BP is characterized by unradiogenic εNd values (-14.1±0.3) and corresponds to a warm period in Europe known as the Roman Warm Period (Moffa-Sánchez et Hall, 2017). The cold periods corresponding to the Dark Ages Cold Period, between 1.2 and 1.7 ka BP, are associated with more radiogenic εNd values (-12.4 to -13.4). The climatic history of Northern Europe before the Roman Warm Period is less clear but the NE Atlantic region did witness a cold event at 2.8-3.5 ka BP (Mayewski et al., 2004; Moffa-Sánchez et Hall, 2017), which is also associated with radiogenic εNd values (-11.9). This extends the chronological framework of the results previously obtained by Copard et al. (2012) on CWC of the SW Rockall Trough and confirms that warm intervals in the NE Atlantic region and in surrounding land masses are associated with greater eastward extension of the SPG, suggesting an intensification of the surface limb of the AMOC. We are not able to provide any additional explanation for the origin of this oceanic variability, which may result from atmospheric reorganization. However, unlike the large-scale mid-Holocene reorganization that could have induced a northward shift of the westerlies and a greater extension of the SPG between 8.8 and 6.8 ka BP, millennial variability in the intensity and position of the westerlies remains a matter of debate.

5.5. Coupling of the mid-SPG dynamics with the low latitudes

The millennial variations in the coral εNd record obtained on the SW Rockall Trough are not well correlated with other SST and SSS records for the NE Atlantic. However, the εNd data correspond to SST variations observed at ODP site 658 in the eastern subtropical Atlantic off the coast of Mauritania (deMenocal et al., 2000) (Fig. 4e). In addition to the mid-Holocene transition observed in both records, the decrease in the coral εNd values suggests a greater eastward extension of the mid-SPG, which is associated with a decrease of the SST at ODP site 658. Hydrographically, these cold SST events could be linked either to an intensification of the Canary Current carrying cold

waters southwards along the western European margin or to an increase in regional upwelling (deMenocal et al., 2000). This link between the high latitude climate and the variations of SST and SSS in the Canary Current has been found as a fingerprint of freshwater release around Greenland in so-called hosing experiments (Swingedouw et al., 2013). This teleconnection is described as being related to the ocean circulation, the Canary Current being described as a freshwater leakage for low SSS from the SPG to the STG. This link is generally consistent with the teleconnection between North African and Northern Europe climates (e.g., Wassenburg et al., 2016). Cold events centered at 0.4, 0.8 and 2.6-3.3 ka BP for ODP Site 658 have been also observed in core OC437-7 24GGC located in a northern position in the Eastern Tropical Atlantic (Morley et al., 2014). These events are associated with a slight decrease in salinity, suggesting that this is not a regional process and may reflect a greater southward heat transfer from high to low latitudes. Thus, we can infer from this correlation between coral εNd values and low latitude SST records that time intervals of intensified mid-SPG and AMOC might correspond to a decrease in the latitudinal thermal gradient in the North Atlantic. This would have led to a major atmospheric reorganization during the mid-Holocene, with a northward shift of the Hadley cell circulation and of the Inter Tropical Convergence Zone (ITCZ), as suggested by modeling studies (Swingedouw et al., 2009; Marshall et al., 2014).

6. Conclusions

In this paper, we have analyzed the radiocarbon content and the Nd isotope composition of precisely U-Th dated fragments of *L. pertusa* and *M. oculata* collected from the SW Rockall Trough margin. These have been combined with previous results for the same region in order to characterize mid-SPG dynamics and their potential impacts on NADW formation and climate in Northern Europe.

The coral εNd record exhibits pronounced variability, ranging from -12.2±0.3 to -16.6±0.4, and tracks the position of the mid-SPG through time. As such, our new record reflects mixing of waters from the SPG (-15) and from the sub-tropical Atlantic (-11) (mainly ENAW and MSW).

The time interval from 8.8 to 6.8 ka BP, which corresponds to the so-called Holocene thermal maximum, has been linked to a greater eastward extension of the mid-SPG and a stronger AMOC. This time interval was followed by a progressive contraction of the SPG between 7 and 5 ka BP. This contraction was associated with a re-organization of thermohaline circulation and a progressive decline in the production of the ISOW in the Nordic Seas during the mid-Holocene and the initiation of LSW formation around 7 ka BP. After 5 ka BP, the CWC εNd value record displays millennial scale variability with a greater eastward extension of the mid-SPG centered at 4.4, 2.5, 1.8 and 0.8 ka BP, corresponding to the warm periods over northern Europe (such as the Medieval Climatic Anomaly and the Roman Warm Period) and coinciding with an intensification of the AMOC. Radiocarbon results show minor $\Delta^{14}C$ depletion (high reservoir ages) around 6.1, 4.4, 2.7, 2 and 0.7-1 ka BP. These

fluctuations, associated with a decrease of the εNd values, may result either from local variability of the mixed layer depth or may be advected from the SPG where deep convection gives rise to relatively $\Delta^{14}C$ depleted thermocline waters.

We suggest that the Early Holocene active state of the SPG intensity could be linked to an entrainment of unradiogenic intermediate water masses originating from the SPG in the northern deep-waters during its overflows from the Nordic Seas. This entrainment could have contributed to the unradiogenic Nd isotopic signature observed for the NADW in the North Atlantic. Further modeling experiments will be necessary to evaluate the impact of this process on the Nd isotopic signature of the deep-water masses of the North Atlantic Ocean.

Overall, we propose that the εNd record for the SW Rockall Trough is a reliable record of SPG extension in the NE Atlantic, independent of the intensity of the inter-gyre mixing. We have identified a correspondence between mid-SPG extension, AMOC intensity and climate in Northern Europe that needs to be further explored.

Acknowledgements

The research leading to this paper was funded by the National Research Agency L-IPSL Project (Grant ANR-10-LABX-0018) and the HAMOC Project (Grant ANR-13-BS06-0003). We would also like to thank the crew, technicians and scientific teams of the MINGULAY-ROCKALL (RV L'Atalante), 64PE360-Corals 2012 and 64PE377-Corals 2013 (RV Pelagia) research cruises for their excellent work during the seawater and CWC sampling. We gratefully acknowledge the support provided by Louise Bordier during Nd isotopic composition analyses and the ^{14}C team of LSCE during physico-chemical treatment of samples prior to ^{14}C measurements. We thank the staff of the AMS-Artemis facility (UMS 2572) who measured ^{14}C. Comments of A.H.L. Voelker as well as the constructive reviews of two anonymous reviewers, considerably helped to improve this manuscript. Furu Mienis is supported financially by the Innovational Research Incentives Scheme of the Netherlands Organisation for Scientific Research (NWO-VENI/VIDI).

Figure captions:

Figure 1: a) Bathymetric maps of the SW Rockall margin showing the locations of the studied cores (Corals2012-39PC, Corals2013-18PC, M2000-25BX) and all other cores discussed in this study. b) North Atlantic currents. The black arrows represent surface and intermediate currents. Dotted lines represent deep circulation. The main water masses are labelled in italics. The gray arrows identify the

main directions of LSW propagation. AAIW, Antarctic Intermediate Water; DSOW, Denmark Strait Overflow Water; ENACW, Eastern North Atlantic Central Water; ISOW, Iceland-Scotland Overflow Water; LDW, Lower Deep Water; LSW, Labrador Sea Water; MSW, Mediterranean Sea Water; NADW, North Atlantic Deep Water; SAIW, Subarctic Intermediate Water; SEC, Shelf Edge Current; WNACW, Western North Atlantic Central Water. Map created with Ocean Data View Software (Schlitzer, R., Ocean Data View, http://odv.awi.de, 2015).

Figure 2: a) Potential temperature (°C), salinity and εNd depth profiles for the water station ICE-CTD-03 located in the Rockall Trough and collected in June and July 2012 during the ICE-CTD cruise on board of the *R/V Thalassa* (Dubois-Dauphin et al., 2017). The water depth of the modern CWC investigated in this study (M2000-25BX) is indicated by a gray horizontal band; b) Maps showing the distribution of the salinity and the seawater εNd in the North Atlantic (Copard et al., 2011; Dubois-Dauphin et al., 2017; Lambelet et al., 2016) as well as a schematic representation of the circulation at 750 m. The salinity distribution at 750 m of water depth has been also reported. The red star indicates the position of the studied sites (locations of cores Corals2012-39PC and Corals2013-18PC). Complete names of water mass accronyms have been provided in Figure 1

Figure 3: a) Comparison of deep-sea coral $\Delta^{14}C$ (‰) with the IntCal13 and Marine13 $\Delta^{14}C$ (‰) calibration curves. The $\Delta^{14}C$ results obtained from CWC in this study are plotted with one item of published data (Frank et al., 2004) against U-Th dates. The uncertainties of $\Delta^{14}C$ and of the U-Th ages are plotted as 2σ error ellipses; b) Li/Mg temperature of CWC from cores Corals2012-39PC (black circle) and Corals2013-18PC (open circle) (Bonneau et al., 2018); c) composite record of CWC εNd obtained from studied cores (cores Corals2012-39PC and Corals2013-18PC) and from previous data obtained from cores MD01-2454G and ENAM9915 (Colin et al., 2010; Copard et al., 2012). Positions of cores have been reported in the Figure 1.

Figure 4: Comparison between the composite record of CWC εNd (f) and (a) $\delta^{18}O_{seawater}$ (‰ SMOW) at Orphan Knoll in the Labrador Sea obtained from $\delta^{18}O$ and Mg/Ca derived T°C analysed on planktonic foraminifera *G. bulloides* (cores HU91-045-093 and MD95-2024, 3488 m) (Hoogakker et al., 2015); (b) Stacked data of SS values obtained from several cores located on the South Iceland Rise and Bjorn Drift. This stacked data of sortable silt (SS) represents the relative strength of the Iceland–Scotland overflow (ISOW) (Thornalley et al., 2013). Higher values for the SS mean size represent an increase in the velocity of the ISOW (e.g. Bianchi and McCave, 1999; Thornalley et al., 2013) ; (c) Salinity of the sub-thermocline water derived from the measurement of Mg/Ca–$\delta^{18}O$ on *G. inflata* in core RAPiD-12-

1K located south of Iceland; (d) Relative abundance of *G. inflata* (%) obtained for cores ENAM33 located east of the Faroe Islands near the Iceland Faroe gap (Staines-Urías et al., 2013); (e) SST anomaly (°C) obtained on ODP site 658 located off Cap Blanc (Mauritania) (deMenocal et al., 2000).

Tables caption:

Table 1: Position, species and U-Th ages (Bonneau et al., 2018) of the deep-sea coral samples investigated in this study. Results of Nd concentrations, Nd isotopic compositions, ^{14}C age, $\Delta^{14}C$ (‰) and marine reservoir ages of the deep-sea coral samples investigated in this study are also presented. $\varepsilon Nd = [(^{143}Nd/^{144}Nd)_{sample}/(^{143}Nd/^{144}Nd)_{CHUR} -1] *10000$, with the present-day $(^{143}Nd/^{144}Nd)_{CHUR}$ value of 0.512638 (Jacobsen and Wasserburg, 1980).

References:

Adkins, J.F., Cheng, H., Boyle, E.A., Drufel, E.R.M., Edwards, R.L., 1998. Deep-sea coral evidence for rapid change in ventilation of the deep North Atlantic 15.400 years ago. Science, 280, 725–728.

Andersen, C., Koc, N., Moros, M., 2004. A highly unstable Holocene climate in the subpolar North Atlantic: evidence from diatoms. Quaternary Science Reviews, 23, 2155–2166.

Ascough, P.L., Cook, G.T., Dugmore, A.J., 2009. North Atlantic marine ^{14}C reservoir effects: Implications for Late-Holocene chronological studies. Quaternary Geochronology, 4(3), 171-180.

Ayache, M., Swingedouw, D., Mary, Y., Eynaud, F., Colin, C., 2018. Multi-centennial variability of the AMOC over the Holocene: A new reconstruction based on multiple proxy-derived SST records. Global and Planetary Change, 170, 172-189.

Bersch, M., 2002. North Atlantic Oscillation-induced changes of the upper layer circulation in the northern North Atlantic Ocean, J. Geophys. Res. 107(C10), 3156, doi:10.1029/2001JC000901.

Berx, B., Payne, M.R., 2017. The Sub-Polar Gyre Index–a community data set for application in fisheries and environment research. Earth System Science Data, 9(1), 259.

Bianchi, G.G., McCave, I.N., 1999. Holocene periodicity in North Atlantic climate and deep ocean flow south of Iceland. Nature 397, 515–517.

Böhm, E., Lippold, J., Gutjahr, M., Frank, M., Blaser, P., Antz, B., Fohlmeister, J., Frank, N., Andersen, M.B., Deininger, M., 2015. Strong and deep Atlantic meridional overturning circulation during the last glacial cycle. Nature, 517, 73–76, doi:10.1038/nature14059.

Bond, G., Showers, W., Cheseby, M., Lotti, R., Almasi, P., de Menocal, P., Priore, P., Cullen, H., Hajdas, I., Bonani, G., 1997. A pervasive millennial-scale cycle in the North Atlantic Holocene and glacial climates. Science, 294, 2130–2136.

Bond, G., Kromer, B., Beer, J., Muscheler, R., Evans, M.N., Showers, W., Hoffmann, S., Lotti-Bond, R., Hajdas, I., Bonani, G., 2001. Persistent solar influence on North Atlantic climate during the Holocene. Science, 278, 1257–1266Bonneau, L., Colin, C., Pons-Branchu, E., Mienis, F., Tisnerat-Laborde, N., Blamart, D., Eliott, M., Collart, T., Frank, N., Foliot, L., Douville, E., 2018. Imprint of Holocene climate variability on cold-water coral reef growth at the SW Rockall Trough margin, NE Atlantic. Geochemistry, Geophysics, Geosystems, DOI: 10.1029/2018GC007502.

Born, A., Stocker, T.F., Sandø, A.B., 2016. Transport of salt and freshwater in the Atlantic Subpolar Gyre, Ocean Dynamics. 66: 1051–1064. doi: 10.1007/s10236-016-0970-y.

Butzin, M., Köhler, P., Lohmann, G., 2017. Marine radiocarbon reservoir age simulations for the past 50,000 years. Geophysical Research Letters, 44(16), 8473-8480.

Came, R.E., Oppo, D.W., McManus, J.F., 2007. Amplitude and timing of temperature and salinity variability in the subpolar North Atlantic over the last 10.000 years. Geology, 35, 315–318.

Carlson, A.E., LeGrande, A.N., Oppo, D.W., Came, R.E., Schmidt, G.A., Anslow, F.S., Licciardi, J.M., Obbink, E.A., 2008. Rapid Early Holocene deglaciation of the Laurentide ice sheet. Nature Geoscience, 1, 620–624.

Carton, J.A., Grodsky, S.A., Liu, H., 2008. Variability of the Oceanic Mixed Layer, 1960–2004. Journal of Climate, 21(5), 1029-1047.

Colin, C., Norbert, N., Copard, K., Douville, E., 2010. Neodymium isotopic composition of deep-sea corals from NE Atlantic : implications for past changes of hydrology during the Holocene. Quaternary Science Reviews, 29, 2509–2517.

Copard, K., Colin, C., Douville, E., Freiwald, A., Gudmundsson, G., de Mol, B., Frank, N., 2010. Nd isotopes in deep-sea corals in the North-eastern Atlantic. Quat. Sci. Rev. 29, 2499–2508.

Copard, K., Colin, C., Frank, N., Reverdin, G., Jeandel, C., Ferron, B., 2011. Nd isotopic composition of water masses and dilution of the Mediterranean outflow along South–West European margin. Geochem. Geophys. Geosyst. 12, Q06020. doi:10.1029/2011GC003529.

Copard, K., Colin, C., Henderson, G.M., Scholten, J., Douville, E., Sicre, M.A., Frank, N., 2012. Late Holocene intermediate water variability in the northeastern Atlantic as recorded by deep-sea corals. Earth Planet. Sci. Lett. 313-314, 34–44.

Cottereau, E., Arnold, M., Moreau, C., Baqué, D., Bavay, D., Caffy, I., Comby, C., Dumoulin, JP., Hain, S., Perron, M., Salomon, J., Setti, V., 2007. Artemis, the new 14C AMS at LMC14 in Saclay, France. Radiocarbon, 49, 291–299.

Crocket, K.C., Vance, D., Gutjahr, M., Foster, G.L., Richards, D., 2011. Persistent Nordic deep-water overflow to the glacial North Atlantic. Geology, 39, 515–518, doi:10.1130/G31677.1.

Curry, R.G., McCartney, M.S., 2001. Ocean gyre circulation changes associated with the North Atlantic Oscillation. J. Phys. Oceanogr. 31, 3374–3400.

de Vernal, A., Hillaire-Marcel, C., 2006. Provincialism in trends and high frequency changes in the northwest North Atlantic during the Holocene. Global and Planetary Change. 54, 263–290.

Debret, M., Bout-Roumazeilles, V., Grousset, F., Desmet, M., McManus, J.F., Massei, N., Sebag, D., Petit, J.R., Copard, Y., Trentesaux, A., 2007. The origin of the 1500-year climate cycles in Holocene North-Atlantic records. Climate of the Past, 3, 569–575.

deMenocal, P., Ortiz, J., Guilderson, T., Sarnthein, M., 2000. Coherent high- and low-latitude climate variability during the Holocene Warm Period. Science, 288, 2198–2202.

Desprat, S., Combourieu-Nebout, N., Essallami, L., Sicre, M, A., Dormoy, I., Peyron, O., Siani, G., Bout Roumazeilles, V., Turon, J, L., 2013. Deglacial and Holocene vegetation and climatic changes in the southern Central Mediterranean from a direct land-sea correlation. Clim. Past. 9, 767–787.

Dubois-Dauphin, Q., Bonneau, L., Colin, C., Montero-Serrano, J.C., Montagna, P., Blamart, D., Hebbeln, D., Van Rooij, D., Pons-Branchu, E., Hemsing, F., Wefing, A.M., Frank, N., 2016. South Atlantic intermediate water advances into the North-east Atlantic with reduced Atlantic meridional overturning circulation during the last glacial period. Geochemistry Geophysics Geosystems, 17(6), 2236–2353.

Dubois-Dauphin, Q., Colin, C., Bonneau, L., Montagna, P., Wu, Q., Van Rooij, D., Reverdin, G., Douville, E., Thil, F., Waldner, A., Frank, N., 2017. Fingerprinting Northeast Atlantic water masses using Neodymium isotopes. Geochimica et Cosmochimica Acta, 210, 267–288.

Eiríksson, J., Knudsen, K.L., Larsen, G., Olsen, J., Heinemeier, J., Bartels-Jónsdóttir, H.B., Jiang, H., Ran, L., Símonarson, L.A., 2011. Coupling of palaeoceanographic shifts and changes in marine reservoir ages off North Iceland through the last millennium. Palaeogeography, Palaeoclimatology, Palaeoecology, 302(1), 95-108.

Ellett, D.J., Edwards, A., Bowers, R., 1986. The hydrography of the Rockall Channel - An overview. Proc. R. Soc. Edinburgh. Sect. B. Biol. Sci, 88, 61–81.

Eynaud, F., Mary, Y., Zumaque, J., Wary, M., Gasparotto, M.-C., Swingedouw, D., Colin, C. 2018. Compiling multiproxy quantitative hydrographic data from Holocene marine archives in the North Atlantic: a way to decipher oceanic and climatic dynamics and natural modes?, Global and Planetary Change, 170; 48-61.

Flatau, M.K., Talley, L., Niiler P.P., 2003. The North Atlantic Oscillation, surface current velocities, and SST changes in the subpolar North Atlantic. Journal of Climate, 16, 2355–2369.

Frank, N., Paterne, M., Ayliffe, L., Van Weering, T., Henriet, J.-P., Blamart, D., 2004. Eastern North Atlantic deep-sea corals : Tracing upper intermediate water $\Delta^{14}C$ during the Holocene. Earth and Planetary Science Letters, 219, 297–309.

Franke, J., Paul, A., Schulz, M., 2008. Modeling variations of marine reservoir ages during the last 45 000 years. Clim. Past, 4(2), 125-136.

García-Ibáñez, M.I., Pardo, P.C., Carracedo, L.I., Mercier, H., Lherminier, P., Ríos, A.F., Pérez, F.F., 2015. Structure, transports and transformations of the water masses in the Atlantic Subpolar Gyre. Prog. Oceanogr. 135, 18–36, doi:10.1016/j.pocean.2015.03.009.

Gastineau, G., L'Heveder, B., Codron, F., Frankignoul, C., 2016. Mechanisms Determining the Winter Atmospheric Response to the Atlantic Overturning Circulation. Journal of Climate, 29 (10), 3767–3785, doi:10.1175/jcli-d-15-10 0326.1.

Hakkinen, S., Rhines P.B., Worthen D.L., 2011. Warm and saline events embedded in the meridional circulation of the northern North Atlantic. J. Geophys. Res. 116, C03006. doi:10.1029/2010JC006275.

Hakkinen, S., Rhines, P.B., 2004. Decline of Subpolar North Atlantic Circulation during the 1990s. Science, 304, 555–559. doi:10.1126/science.1094917.

Hátún, H., Sandø, A.B., Drange, H., Hansen, B., Valdimarsson, H., 2005. Influence of the Atlantic subpolar gyre on the thermohaline circulation. Science, 309, 1841–1844.

Hillaire-Marcel, C., de Vernal, A., Bilodeau, G., Weaver, A.J., 2001. Absence of deep-water formation in the Labrador Sea during the last interglacial period. Nature, 410, 1073–1077.

Holliday, N.P., Pollard, R.T., Read, J.F., Leach, H., 2000. Water mass properties and fluxes in the Rockall Trough, 1975 - 1998. Deep-Sea Research, 47, 1303–1332.

Hoogakker, B.A., McCave, I.N., Elderfield, H., Hillaire-Marcel, C., Simstich, J., 2015. Holocene climate variability in the Labrador Sea. Journal of the Geological Society, 172, 272–277.

Hoogakker, B.A.A., Chapman, M.R., McCave, I.N., Hillaire-Marcel, C., Ellison, C.R.W., Hall, I.R., Telford, R.J., 2011. Dynamics of North Atlantic Deep Water masses during the Holocene. Paleoceanography, 26, 1–10.

Howe, J., Piotrowski, A.M., Rennie, V., 2016. Abyssal origin for the Early Holocene pulse of unradiogenic neodymium isotopes in Atlantic seawater. Geology, 44, 831-834. https://doi.org/10.1130/G38155.1.

Jacobsen, S.B., Wasserburg, G.J., 1980. Sm-Nd isotopic evolution of chondrites. Earth and Planetary Science Letters, 50, 139–155.

Jeandel, C., Arsouze, T., Lacan, F., Techine, P., Dutay, J.C., 2007. Isotopic Nd compositions and concentrations of the lithogenic inputs into the ocean: A compilation. with an emphasis on the margins. Chem. Geol. 239, 156–164.

Key, R.M., Kozyr, A., Sabine, C.L., Lee, K., Wanninkhof, R., Bullister, J.L., Feely, R.A., Millero, F.J., Mordy, C., Peng, T.H., 2004. A global ocean carbon climatology: Results from Global Data Analysis Project (GLODAP). Global Biogeochemical Cycles, 18(4).

Kissel, C., Van Toer, A., Laj, C., Cortijo, E., Michel, E., 2013. Variations in the strength of the North Atlantic bottom water during Holocene. Earth and Planetary Science Letters, 369, 248–259.

Kurzweil, F., Gutjahr, M., Vance, D., Keigwin, L., 2010. Authigenic Pb isotopes from the Laurentian Fan: changes in chemical weathering and patterns of North American freshwater runoff during the last deglaciation. Earth and Planetary Science Letters, 299, 458-465.

Lacan, F., Jeandel, C., 2004. Subpolar Mode Water formation traced by neodymium isotopic composition. Geophys. Res. Let. 31, L14306.

Lacan, F., Jeandel, C., 2005. Acquisition of the neodymium isotopic composition of the North Atlantic Deep Water. Geochemistry Geophysics Geosystems, 6, 12, Q12008. doi: 10.1029/2005GC000956.

Lambelet, M., van de Flierdt, T., Crocket, K., Rehkämper, M., Kreissig, K., Coles, B., Rijkenberg, M.J.A., Gerringa, L.J.A., de Baar, H.J.W., Steinfeldt, R., 2016. Neodymium isotopic composition and concentration in the western North Atlantic Ocean: Results from the GEOTRACES GA02 section. Geochim. Cosmochim. Acta. 177, 1–29. doi:10.1016/j.gca.2015.12.019.

Larsen, D.J., Miller, G.H., Geirsdottir, A., 2013. Asynchronous Little Ice Age glacier fluctuations in Iceland and European Alps linked to shifts in subpolar North Atlantic circulation. Earth and Planetary Science Letters, 380, 52–59.

Lavender, K.L., Brechner Owens, W., Davis, R.E., 2005. The mid-depth circulation of the subpolar North Atlantic Ocean as measured by subsurface floats. Deep. Res. Part I Oceanogr. Res. Pap. 52, 767–785. http://dx.doi.org/10.1016/j.dsr.2004.12.007.

Lippold, J., Gutjahr, M., Blaser, P., Christner, E., Carvalho Ferreira, M-L., Mulitza, S., Christl, M., Wombacher, F., Böhm, E., Antz, B., Cartapanis, O., Vogel, H., Jaccard, S., 2016. Deep water provenance and dynamics of the (de)glacial Atlantic meridional overturning circulation. Earth Planet. Sci. Lett. 445, 68–78.

Lozier, M.S., Stewart, N.M., 2008. On the Temporally Varying Northward Penetration of Mediterranean Overflow Water and Eastward Penetration of Labrador Sea Water. J. Phys. Oceanogr. 38, 2097–2103.

Lugmair, G.W., Shimamura, T., Lewis, R.S., Anders, E., 1983. Samarium-146 in the Early Solar System: Evidence from Neodymium in the Allende Meteorite. Science, 222, 1015–1018.

Marchal, O., Cacho, I., Stocker, T.F., Grimalt, J.O., Calvo, E., Martrat, B., Shackleton, N., Vautravers, M., Cortijo, E., van Kreveld, S., Andersson, C., Koc, N., Chapman, M., Sbaffi, L., Duplessy, J.-C., Sarnthein, M., Turon, J.-L., Duprat, J., Jansen, E., 2002. Apparent long-term cooling of the sea surface in the northeast Atlantic and Mediterranean during the Holocene. Quaternary Science Reviews, 21, 455–483.

Marshall, J., Donohoe, A., Ferreira, D., McGee, D., 2014. The ocean's role in setting the mean position of the Inter-Tropical Convergence Zone. Climate Dynamics, 42 (7-8), 1967–1979. doi :10.1007/s00382-013-1767-z.

865 Mary, Y., Eynaud, F., Colin, C., Rossignol, L., Brocheray, S., Mojtahid, M., Garcia, J., Peral, M., Howa,
866 H., Zaragosi, S., Cremer, M., 2017. Changes in Holocene meridional circulation and poleward Atlantic
867 flow: the Bay of Biscay as a nodal point. Clim. Past. 13, 201–216, doi:10.5194/cp-13-201-2017.

868 Mayewski, P.A., Rohling, E.E., Stager, J.C., Karlén, W., Maasch, K.A., Meeker, L.D., Meyerson, E.A.,
869 Gasse, F., van Kreveld, S., Holmgren, K., Lee-Thorp, J., Rosqvist, G., Rack, F., Staubwasser, M.,
870 Schneider, R.R., Steig, E.J., 2004. Holocene climate variability. Quaternary Research. 62(3), 243–255.

871 Mienis, F., De Stigter, H.C., White, M., Duineveld, G., De Haas, H., Van Weering, T.C.E., 2007.
872 Hydrodynamic controls on cold-water coral growth and carbonate-mound development at the SW
873 and SE Rockall Trough Margin, NE Atlantic Ocean. Deep-Sea Res. Pt. I. 54, 1655–1674.

874 Mienis, F., Van Weering, T., De Haas, H., De Stigter, H., Huvenne, V., Wheeler, A., 2006. Carbonate
875 mound development at the SW Rockall Trough margin based on high resolution TOBI and seismic
876 recording. Mar. Geol. 233, 1–19.

877 Miettinen, A., Divine, D.V., Koc, N., Godtliebsen, F., Hall, I.R., 2012. Multicentennial variability of the
878 sea surface temperature gradient across the subpolar North Atlantic over the last 2.8 kyr. Journal of
879 Climate, 4205–4219.

880 Moffa-Sánchez, P., Hall, I.R., 2017. North Atlantic variability and its links to European climate over the
881 last 3000 years. Nature Communications, 8, 1–9.

882 Mohn, C., Rengstorf, A., White, M., Duineveld, G., Mienis, F., Soetaert, K., Grehan, A., 2014. Linking
883 benthic hydrodynamics and cold-water coral occurrences: A high-resolution model study at three
884 cold-water coral provinces in the NE Atlantic. Progress In Oceanography, 122, 92–104.

885 Montero-Serrano, J.-C., Frank, N., Colin, C., Wienberg, C., Eisele, M., 2011. The climate influence on
886 the mid-depth Northeast Atlantic gyres viewed by cold-water corals. Geophys. Res. Lett. 38,
887 doi:10.1029/2011GL048733.

888 Montero-Serrano, J.-C., Frank, N., Tisnérat-Laborde, N., Colin, C., Wu, C., Lin, K., Shen, C., Copard, K.,
889 Orejas, C., Gori, A., De Mol, L., Van Rooij, D., Reverdin, G., Douville, E., 2013. Decadal changes in the
890 mid-depth water mass dynamic of the Northeastern Atlantic margin (Bay of Biscay). Earth Planet. Sci.
891 Lett. 364, 134–144.

892 Morley, A., Rosenthal, Y., deMenocal, P., 2014. Ocean-atmosphere climate shift during the mid-to-
893 late Holocene transition. Earth and Planetary Sciences Letters, 388, 18–26.

894 New, A.L., Smythe-Wright, D., 2001. Aspects of the circulation in the Rockall Trough. Cont. Shelf Res.
895 21, 777–810.

896 O'Brien, S.R., Mayewski, P.A., Meeker, L.D., Meese, D.A., Twickler, M.S., Witlow, S.I., 1995.
897 Complexity of Holocene climate as reconstructed from a Greenland ice core. Science, 270, 962–964.

898 Ortega, P., Lehner, F., Swingedouw, D., Masson-Delmotte, V., Raible, C.C., Casado, M., Yiou P., 2015.
899 A multi-proxy model-tested North Atlantic Oscillation reconstruction for the last millennium. Nature
900 523, 71–74, doi:10.1038/nature14518.

901 Piepgras, D.J., Wasserburg, G.J., 1987. Rare earth element transport in the western North Atlantic
902 inferred from Nd isotopic observations. Geochim. Cosmochim. Acta. 51, 1257–1271.

903 Pollard, R.T., Gritths, M.J., Cunningham, S.A., Read, J.F., Perez, F.F., Rios, A.F., 1996. Vivaldi 1991 - a
904 study of the formation. circulation and ventilation of Eastern North Atlantic Central Water. Progr.
905 Oceanogr. 37, 167–172.

906 Praetorius, S., McManus, J., Oppo, D., Curry, W., 2008. Episodic reductions in bottom-water currents
907 since the last ice age, Nature Geoscience, 1, 449-452.

Rasmussen, T.L., Bäckström, D., Heinemeier, J., Klitgaard-Kristensen, D., Knutz, P.C., Kuijpers, A., Lassen, S., Thomsen, E., Troelstra, S.R., van Weering, T.C.E., 2002. The Faroe-Shetland Gateway: Late Quaternary water mass exchange between the Nordic seas and the northeastern Atlantic. Mar. Geol. 188, 165–192.

Reimer, P.J., Bard, E., Bayliss, A., Beck, J.W., Blackwell, P.G., Bronk Ramsey, C., Buck, C.E, Cheng, H., Edwards, R.L, Friedrich, M., Grootes, P.M., Guilderson, TP., Haflidason, H., Hajdas, I., Hatté, C., Heaton, T.J., Hoffmann, D.L., Hogg, A.G., Hughen, K.A., Kaiser, K.F, Kromer, B., Manning, S.W., Niu, M., Reimer, R.W., Richards, D.A., Scott, E.M., Southon, J.R., Staff, R.A., Turney, C.S.M., van der Plicht, J., 2013. Intcal13 and Marine13 radiocarbon age calibration curves 0-50,000 years cal BP. Radiocarbon, 55(4), 1869–1887.

Renssen, H., Goosse, H., Fichefet, T., 2005. Contrasting trends in North Atlantic deep-water formation in the Labrador Sea and Nordic Seas during the Holocene. Geophysical Research Letters, 32, L08711. doi:10.1029/2005GL022462.

Renssen, H., Seppä, H., Heiri, O., Roche, D.M., Goosse, H., Fichefet, T., 2009. The spatial and temporal complexity of the Holocene thermal maximum. Nature Geoscience, 2, 411–414.

Repschläger, J., Garbe-Schönberg, D., Weinelt, M., Schneider, R., 2017, Holocene evolution of the North Atlantic subsurface transport, Clim. Past, 13, 333–344.

Reverdin, G., Cayan, D., Kushnir, Y., 1997. Decadal variability of hydrography in the upper northern North Atlantic in 1948-1990. Journal of Geophysical Research, 102 (C4), 8505–8531.

Rickli, J., Frank, M., Halliday, A.N., 2009. The hafnium-neodymium isotopic composition of Atlantic seawater. Earth Planet. Sci. Lett. 280, 118–127.

Roberts, N., Piotrowski, A., McManus, J., Keigwin, L., 2010. Synchronous Deglacial Overturning and Water Mass Source Changes. Science, 327, 75-78.

Sarnthein, M., van Kreveld, S., Erlenkeuser, H., Grootes, P.M., Kucera, M., Pflaumann, U., Schulz, M., 2003. Centennial-to-millennial-scale periodicities of Holocene climate and sediment injections off the western Barents shelf, 75°N. Boreas, 32, 447-461.

Smith, A.C., Wynn, P.M., Barker, P.A., Leng, M.J., Stephen R. Noble, S.R., Tych, W., 2016. North Atlantic forcing of moisture delivery to Europe throughout the Holocene. Scientific Reports, 6:24745, DOI: 10.1038/srep24745.

Sgubin, G., Swingedouw, D., Drijfhout, S., Mary, Y., Bennabi, A., 2017. Abrupt cooling over the North Atlantic in modern climate models. Nature Communications, 8, no 14375.

Solignac, S., de Vernal, A., Hillaire-Marcel, C., 2004. Holocene sea-surface conditions in the North Atlantic - contrasted trends and regimes in the western and eastern sectors (Labrador Sea vs. Iceland Basin). Quaternary Science Reviews, 23, 319–334.

Solignac, S., Giraudeau, J., de Vernal, A., 2006. Holocene sea surface conditions in the western North Atlantic: spatial and temporal heterogeneities. Paleoceanography, 21, 1–16.

Sorrel, P., Debret, M., Billeaud, I., Jaccard, S.L., McManus, J.F., Tessier, B., 2012. Persistent non-solar forcing of Holocene storm dynamics in coastal sedimentary archives. Nat. Geosci. 12, 892–896, doi:10.1038/ngeo1619.

Spielhagen, RF, Werner, K, Sørensen, SA, Zamelczyk, K, Kandiano, E, Budeus, G, Husum, K, Marchitto, TM, Hald, M., 2011. Enhanced modern heat transfer to the Arctic by warm Atlantic Water. Science, 331, 450-453.

Staines-Urías, F., Kuijpers, A., Korte, C., 2013. Evolution of subpolar North Atlantic surface circulation since the Early Holocene inferred from planktic foraminifera faunal and stable isotope records. Quaternary Sci. Rev. 76, 66–81.

Struve, T., van de Flierdt, T., Burke, A., Robinson, L.F., Hammond, S.J., Crocket, K.C., Bradt- miller, L.I., Auro, M.E., Mohamed, K.J., White, N.J., 2017. Neodymium Isotopes and Concentrations in Aragonitic Scleractinian Cold-Water Coral Skeletons - Modern Calibration and Evaluation of Palaeo-Applications. Chemical Geology, 453, 146–168.

Stuiver, M., Polach, H.A., 1977. Discussion reporting of ^{14}C data, Radiocarbon. 19, 355–363.

Swingedouw, D., Mignot, J., Braconnot, P., Mosquet, E., Kageyama, M., Alkama, R., 2009. Impact of freshwater release in the north Atlantic under different climate conditions in an OAGCM. Journal of Climate, 22(23), 6377–6403.

Swingedouw, D., Ortega, P., Mignot, J., Guilyardi, E., Masson-Delmotte, V., Butler, G., Khodri M., 2015. Bidecadal North Atlantic ocean circulation variability controlled by timing of volcanic eruptions. Nature Communications, 6, DOI: 10.1038/ncomms7545.

Swingedouw, D., Rodehacke, C., Behrens, E., Menary, M., Olsen, S., Gao, Y., Mikolajewicz, U., Mignot, J., Biastoch, A., 2013. Decadal fingerprints of fresh water discharge around Greenland in a multi-models ensemble. Climate Dynamics, 41, 695–720, DOI: 10.1007/s00382-012-1479-9.

Thornalley, D.J.R., Blaschek, M., Davies, F.J., Praetorius, S., Oppo, D.W., McManus, J.F., Hall, I.R., Kleiven, H., Renssen, H., McCave, I.N., 2013. Long-term variations in Iceland–Scotland overflow strength during the Holocene. Clim. Past, 9, 2073-2084.

Thornalley, D.J., Elderfield, H., McCave, N., 2009. Holocene oscillations in temperature and salinity of the surface subpolar North Atlantic. Nature, 457, 711–714.

Tisnérat-Laborde, N., Poupeau, J.-J., Tannau, J.-F., Paterne, M., 2001. Development of a semi-automated system for routine preparation of carbonate sample. Radiocarbon, 43(2A), 299–304.

Tisnérat-Laborde, N., Paterne, M., Métivier, B., Arnold, M., Yiou, P., Blamart, D., Raynaud, S., 2010. Variability of the northeast Atlantic sea surface $\Delta^{14}C$ and marine reservoir age and the North Atlantic Oscillation (NAO). Quaternary Science Reviews, 29, 2633–2646.

van de Flierdt, T., Robinson, L.F., Adkins, J. F., Hemming, S.R., Goldstein, S.L., 2006. Temporal stability of the neodymium isotope signature of the Holocene to Glacial North Atlantic. Paleoceanography, 21, doi:10.1029/2006PA001294.

van de Flierdt, T., Robinson, L.F., Adkins, J.F., 2010. Deep-sea corals aragonite as a recorder for the neodymium isotopic composition of seawater. Geochim. Cosmochim. Acta. 74, 6014–6032.

van Haren, H., Mienis, F., Duineveld, G.C., Lavaleye, M.S., 2014. High-resolution temperature observations of a trapped non linear diurnal tide influencing cold-water corals on the Logachev mounds. Progr. Oceanogr. 125, 16–25.

Van Weering, T.C.E., De Haas, H., De Stigter, H.C., Lykke-Andersen, H., Kouvaev, I., 2003. Structure and development of giant carbonate mounds at the SW and SE Rockall Trough margins, NE Atlantic Ocean. Marine Geology. 198, 67–81.

Wanamaker, A.D., Butler, P.G., Scourse, J.D., Heinemeier, J., Eiríksson, J., Knudsen, K.L., Richardson, C., 2012. Surface changes in the North Atlantic meridional overturning circulation during the last millennium. Nature Communications, 3, doi :10.1038/ncomms1901.

Wassenburg, J.A., Dietrich, S., Fietzke, J., Fohlmeister, J., Jochum, K.P., Scholz, D., Richter, D.K., Sabaoui, A., Spotl, C., Lohmann, G., Andreae, M.O., Immenhauser, A., 2016. Reorganization of the North Atlantic Oscillation during Early Holocene deglaciation. Nat. Geosci. 9, 602–605.

White, M., B. Dorschel., 2010. The importance of the permanent thermocline to the cold water coral carbonate mound distribution in the NE Atlantic. Earth and Planetary Science Letters, 296, 395–402.

Wilson, D.J., Crocket, K.C., van de Flierdt, T., Robinson, L.F., Adkins J.F., 2014. Dynamic intermediate ocean circulation in the North Atlantic during Heinrich Stadial 1: A radiocarbon and neodymium isotope perspective. Paleoceanography, 29, 1072–1093. doi:10.1002/2014PA002674.

Zunino, P., Lherminier, P., Mercier, H., Daniault, N., García-Ibáñez, M.I., Pérez, F.F, 2017. The GEOVIDE cruise in May–June 2014 reveals an intense Meridional Overturning Circulation over a cold and fresh subpolar North Atlantic. Biogeosciences, 14, 5323–5342. doi: 10.5194/bg-14-5323-2017.

Table 1

Depth (cm)	Species	$^{230}Th/^{234}U$ Age Cal (ka BP)		Nd (ppb)	$^{143}Nd/^{144}Nd$	± 2σ	εNd	± 2σ	^{14}C age (yr BP) ± 1σ	$\Delta^{14}C$(‰) ± 1σ	MRE (yr ± 1σ)
Coral2012-39PC (55.452N - 15.870W; 742 m water depth)											
0.5	*L. pertusa*	0.251	±0.014	41.3	0.511974	±0.000015	-13.0	±0.3			
1.5	*M. oculata*	0.276	±0.006	16.5	0.511995	±0.000028	-12.5	±0.5	750 ±30	-58±3	571±25
4.5	*M. oculata*	0.473	±0.079		0.511998	±0.000010	-12.5	±0.2			
9.5	*L. pertusa*	0.663	±0.320		0.512014	±0.000014	-12.2	±0.3			
10.5	*M. oculata*	0.606	±0.036	22.0	0.511975	±0.000025	-12.9	±0.5	1120 ±30	-64±6	527±25
15.5	*M. oculata*	0.740	±0.011	13.6	0.512007	±0.000024	-12.3	±0.5			
17.5	*L. pertusa*	0.719	±0.009	8.8	0.511987	±0.000018	-12.7	±0.4			
26.5	*L. pertusa*	0.854	±0.008	8.0	0.512005	±0.000024	-12.3	±0.5			
38.5	*L. pertusa*	1.020	±0.012	12.0	0.511963	±0.000019	-13.2	±0.4	1590 ±30	-72±4	455±25
49.5	*L. pertusa*	1.475	±0.271		0.511983	±0.000010	-12.8	±0.2			
51.5	*L. pertusa*	1.447	±0.014	8.1	0.512000	±0.000024	-12.5	±0.5	1975 ±30	-68±4	387±25
58.5	*L. pertusa*	1.431	±0.014	7.1	0.511982	±0.000018	-12.8	±0.4			
64.5	*M. oculata*	1.427	±0.017	13.4	0.511966	±0.000018	-13.1	±0.4			
73.5	*M. oculata*	1.854	±0.017	17.0	0.511913	±0.000018	-14.1	±0.4			
87.5	*L. pertusa*	2.008	±0.015	28.1	0.511965	±0.000014	-13.1	±0.3	2510 ±30	-67±5	430±30
98.5	*M. oculata*	2.214	±0.010	7.2					2575 ±30	-51±4	334±30
99.5	*M. oculata*	2.370	±0.029	13.5	0.511985	±0.000022	-12.7	±0.4	2660 ±30	-43±6	244±30
105.5	*M. oculata*	2.308	±0.010	14.7	0.511939	±0.000019	-13.6	±0.4			
109.5	*M. oculata*	2.530	±0.015	16.8	0.511912	±0.000024	-14.2	±0.5	2910 ±30	-55±5	423±30
120.5	*M. oculata*	2.786	±0.016	9.1	0.511956	±0.000019	-13.3	±0.4	3195 ±30	-59±5	485±30
137.5	*L. pertusa*	3.673	±0.017	45.0	0.511959	±0.000011	-13.2	±0.2	3580 ±30	-1.6±5	179±30
142.5	*M. oculata*	3.581	±0.015	11.0	0.511932	±0.000018	-13.8	±0.4	3745 ±30	-33±4	395±25
149.5	*L. pertusa*	3.771	±0.069		0.511979	±0.000010	-12.8	±0.2			
151.5	*L. pertusa*	3.797	±0.014	24.5	0.511953	±0.000016	-13.4	±0.3	3865 ±30	-21±5	377±30
169.5	*M. oculata*	4.436	±0.023	46.9	0.511906	±0.000011	-14.3	±0.2	4485 ±30	-21±6	495±30
174.5	*L. pertusa*	4.527	±0.021	42.2	0.511927	±0.000014	-13.9	±0.3	4420 ±30	-3±6	369±30
176.5	*M. oculata*	4.884	±0.020	11.1	0.511949	±0.000023	-13.4	±0.5			
198.5	*L. pertusa*	5.430	±0.039	27.3	0.511934	±0.000024	-13.7	±0.5	4990 ±30	37±8	361±30

199.5	*M. oculata*	4.998	±0.228		0.511955	±0.000010	-13.3	±0.2			
209.5	*M. oculata*	5.258	±0.019								
217.5	*M. oculata*	6.023	±0.024	11.5	0.511897	±0.000018	-14.5	±0.4	5575 ±30	35±6	262±30
227.5	*L. pertusa*	6.110	±0.038	27.8	0.511930	±0.000024	-13.8	±0.5			
235.5	*L. pertusa*	6.126	±0.022	15.6	0.511907	±0.000018	-14.3	±0.4	5820 ±30	14±8	517±40
241.5	*L. pertusa*	6.085	±0.017	8.8	0.511906	±0.000018	-14.3	±0.4	5805 ±30	13±6	519±35
251.5	*M. oculata*	6.670	±0.025	12.0	0.511889	±0.000024	-14.6	±0.5	6240 ±30	31±7	377±40
261.5	*M. oculata*	7.276	±0.033	12.9							
265.5	*M. oculata*	7.562	±0.037	16.3	0.511851	±0.000021	-15.4	±0.4	6984 ±30	46±8	344±35
282.5	*M. oculata*	8.680	±0.029	17.0	0.511869	±0.000022	-15.0	±0.4	8185 ±35	31±8	282±40
297.5	*M. oculata*	9.144	±0.031	21.3	0.511875	±0.000026	-14.9	±0.5	8460 ±35	54±8	230±40
307.5	*L. pertusa*	9.421	±0.057		0.511906	±0.000024	-14.3	±0.5			
323.5	*M. oculata*	9.895	±0.032		0.511912	±0.000024	-14.2	±0.5	9068 ±35	70±9	250±40
332.5	*M. oculata*	10.079	±0.053	76.9	0.511871	±0.000011	-15.0	±0.2	9325 ±35	60±12	457±40
349.5	*L. pertusa*	10.024	±0.324								
354.5	*M. oculata*	10.105	±0.029	13.7	0.511871	±0.000024	-15.0	±0.5	9270 ±35	70±9	419±45
359.5	*M. oculata*	10.752	±0.047		0.511960	±0.000011	-13.2	±0.2			
Corals2013-18PC (55.523N - 15.644W; 790 m water depth)											
27.5	*L. pertusa*	1.293	±0.033		0.512659	±0.000021	-13.0	±0.4			
92.5	*L. pertusa*	3.694	±0.017	23.0	0.512651	±0.000013	-13.6	±0.2			
146.5	*L. pertusa*	5.227	±0.023	25.0	0.512652	±0.000014	-14.1	±0.3			
178.0	*L. pertusa*	5.436	±0.056	22.4	0.512653	±0.000018	-13.7	±0.4			
247.5	*L. pertusa*	6.069	±0.026	22.2	0.512653	±0.000018	-13.9	±0.4			
288.5	*L. pertusa*	6.528	±0.078	45.3	0.512648	±0.000014	-13.9	±0.3			
339.0	*L. pertusa*	7.175	±0.038	35.4	0.512650	±0.000014	-15.4	±0.3			
359.0	*L. pertusa*	7.595	±0.036	55.0	0.512649	±0.000014	-15.4	±0.3			
392.0	*L. pertusa*	8.650	±0.089	10.7	0.512653	±0.000018	-16.6	±0.4			
M2000-25BX											
Top	*L. pertusa*	Living	coral	9.7	0.511937	±0.000018	-13.6	±0.4			

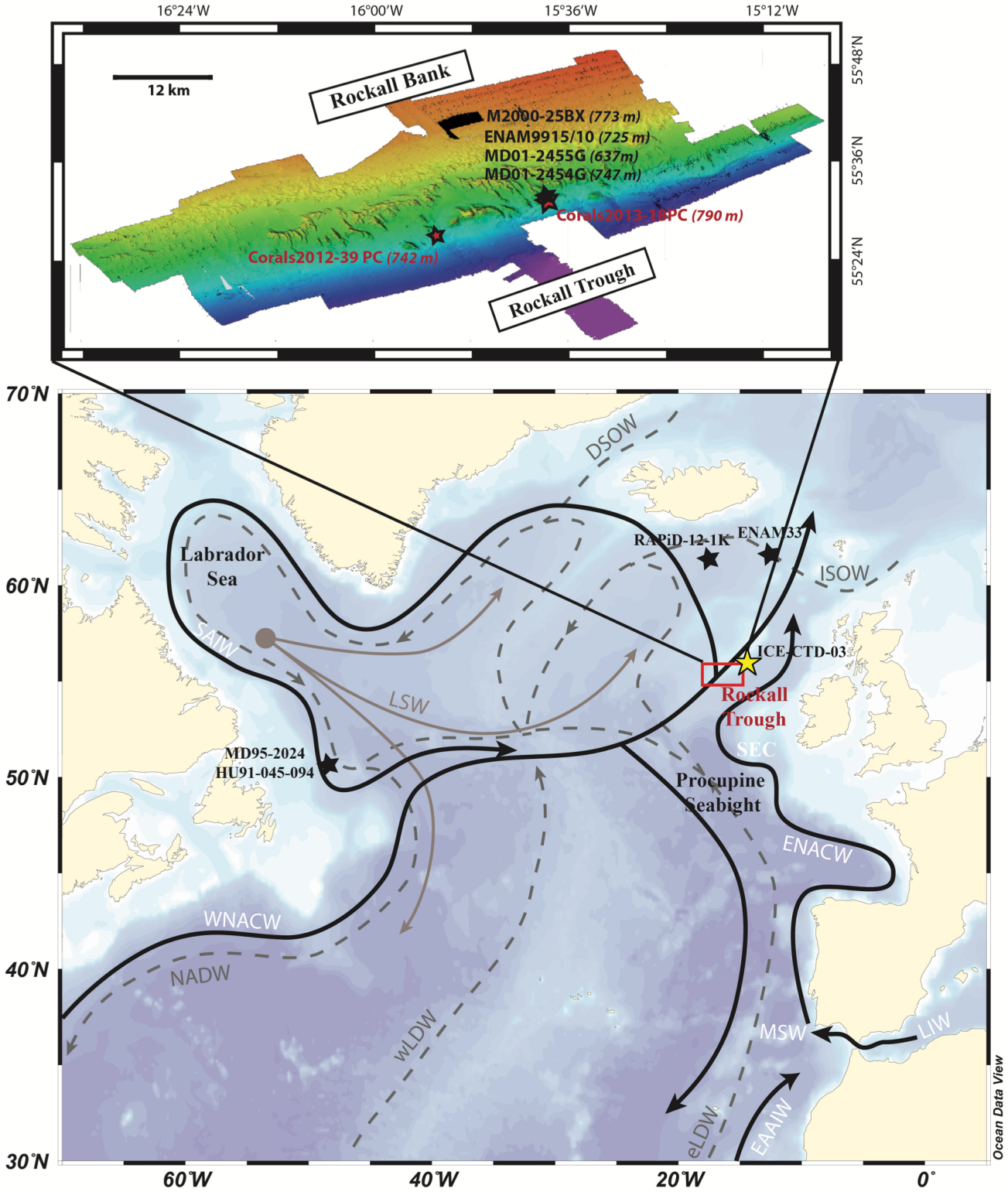
16°24′W
16°00′W
15°36′W
15°12′W
55°48′N
55°36′N
55°24′N
12 km
Rockall Bank
M2000-25BX (773 m)
ENAM9915/10 (725 m)
MD01-2455G (637m)
MD01-2454G (747 m)
Corals2013-18PC (790 m)
Corals2012-39 PC (742 m)
Rockall Trough
70°N
60°N
50°N
40°N
30°N
60°W
40°W
20°W
0°
DSOW
Labrador Sea
SAIW
LSW
RAPiD-12-1K
ENAM33
ISOW
ICE-CTD-03
Rockall Trough
SEC
Procupine Seabight
MD95-2024
HU91-045-094
ENACW
WNACW
NADW
wLDW
eLDW
MSW
LIW
EAAIW
Ocean Data View

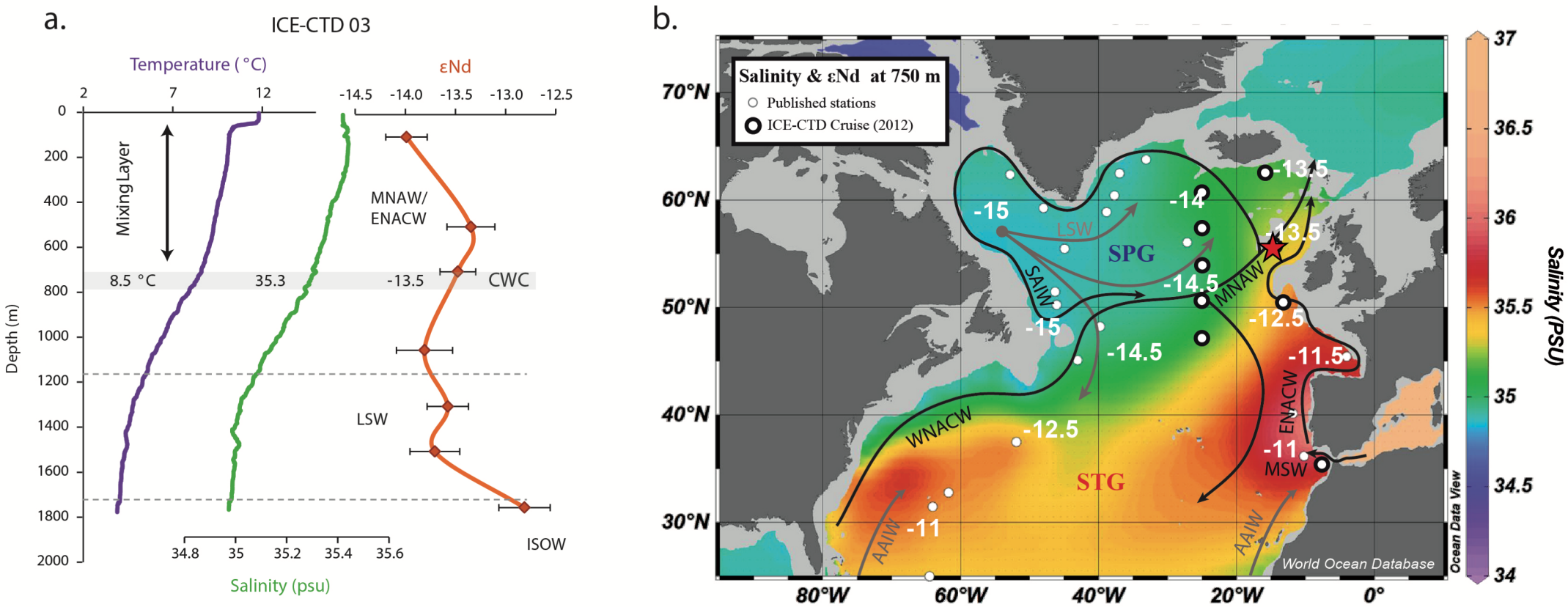
a.
ICE-CTD 03
Temperature (°C)
εNd
2
7
12
-14.5
-14.0
-13.5
-13.0
-12.5
0
200
400
600
800
1000
1200
1400
1600
1800
2000
Depth (m)
Mixing Layer
MNAW/
ENACW
8.5 °C
35.3
-13.5
CWC
LSW
ISOW
34.8
35
35.2
35.4
35.6
Salinity (psu)
b.
Salinity & εNd at 750 m
Published stations
ICE-CTD Cruise (2012)
70°N
60°N
50°N
40°N
30°N
80°W
60°W
40°W
20°W
0°
-15
LSW
SPG
-14
-13.5
-14.5
MNAW
-12.5
-15
-14.5
-11.5
ENACW
WNACW
-12.5
-11
MSW
STG
AAIW
-11
AAIW
SAIW
World Ocean Database
Ocean Data View
37
36.5
36
35.5
35
34.5
34
Salinity (PSU)

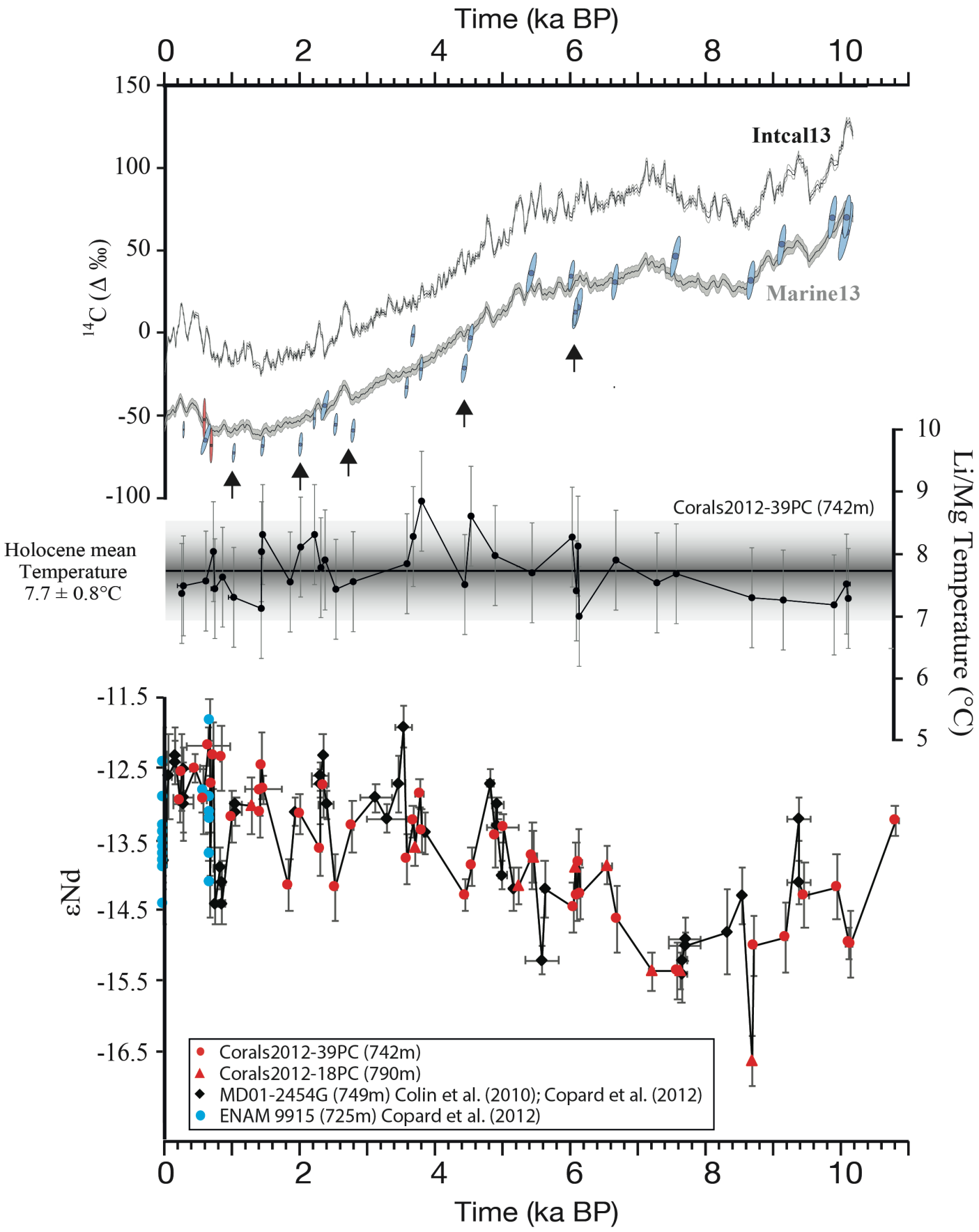
Time (ka BP)
0
2
4
6
8
10
150
100
50
0
-50
-100
^{14}C (Δ ‰)
Intcal13
Marine13
Corals2012-39PC (742m)
Holocene mean
Temperature
7.7 ± 0.8°C
10
9
8
7
6
5
Li/Mg Temperature (°C)
-11.5
-12.5
-13.5
-14.5
-15.5
-16.5
εNd
Corals2012-39PC (742m)
Corals2012-18PC (790m)
MD01-2454G (749m) Colin et al. (2010); Copard et al. (2012)
ENAM 9915 (725m) Copard et al. (2012)
Time (ka BP)

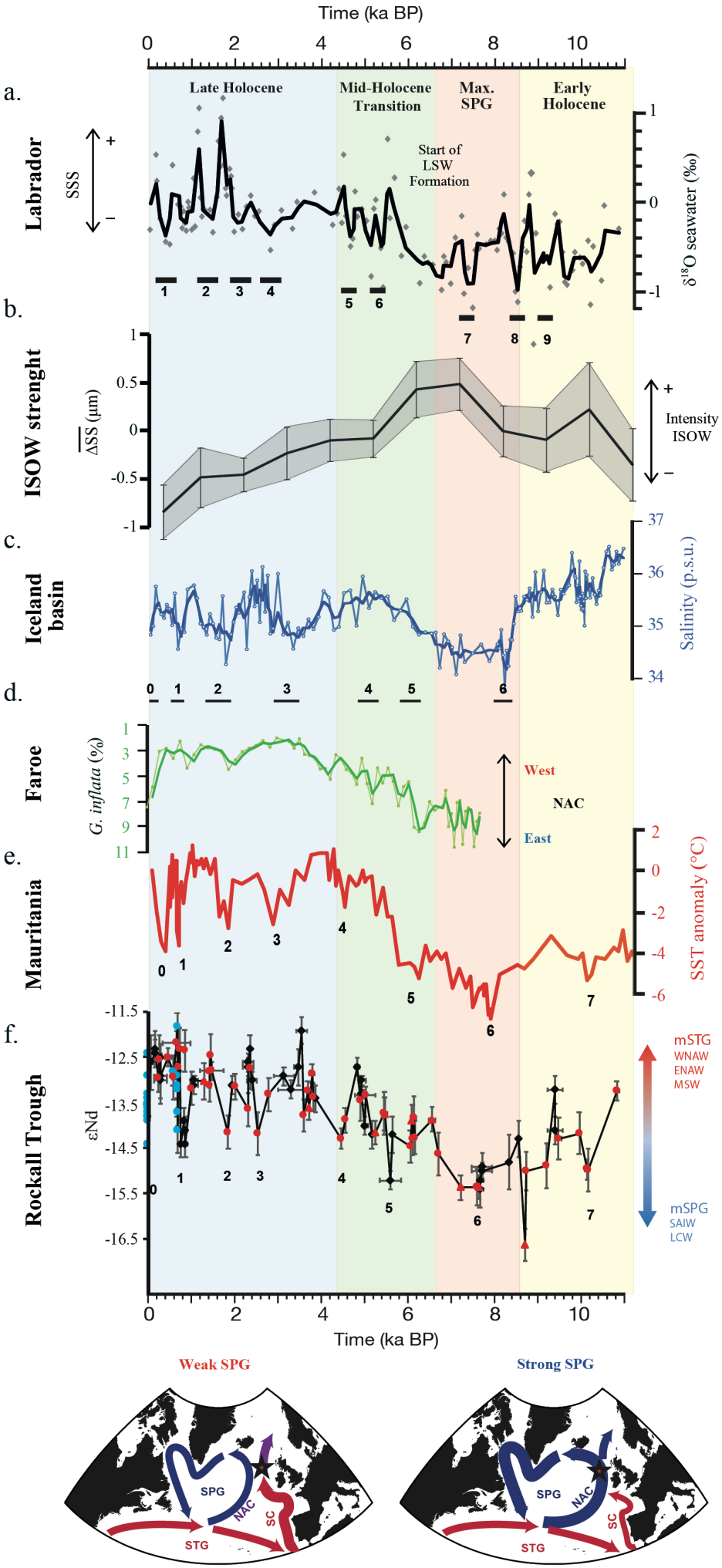
Time (ka BP)
0
2
4
6
8
10
a.
Labrador
SSS
+
–
Late Holocene
Mid-Holocene Transition
Max. SPG
Early Holocene
Start of LSW Formation
1
2
3
4
5
6
7
8
9
δ18O seawater (‰)
b.
ISOW strenght
ΔSS (μm)
Intensity ISOW
c.
Iceland basin
Salinity (p.s.u.)
d.
Faroe
G. inflata (%)
West
NAC
East
e.
Mauritania
SST anomaly (°C)
f.
Rockall Trough
εNd
mSTG
WNAW
ENAW
MSW
mSPG
SAIW
LCW
Time (ka BP)
Weak SPG
Strong SPG
SPG
NAC
SC
STG